European Journal of Immunology Clinical·Basic·Translational

Immunodeficiencies and autoimmunity

Basic

Research Article

High sensitivity of host Helios^{+}/Neuropilin-1^{+} Treg to pretransplant conditioning hampers development of OX40^{bright}/integrin-β7^{+} regulatory cells in acute gastrointestinal GvHD

Nikolett Lupsa[1], Barbara Érsek[1], Csenge Böröczky[1], Dávid Kis[2], Eszter Szarka[2], Katalin Lumniczky[2], Géza Sáfrány[2], Zoltán S Zádori[3], Árpád Szöőr[4], Edit I Buzás[1,5,6] and Zoltán Pós[1]

[1] Department of Genetics, Cell and Immunobiology, Faculty of Medicine, Semmelweis University, Budapest, Hungary
[2] Unit of Radiation Medicine, Department of Radiobiology and Radiohygiene, National Public Health Center, Budapest, Hungary
[3] Department of Pharmacology and Pharmacotherapy, Faculty of Medicine, Semmelweis University, Budapest, Hungary
[4] Department of Biophysics and Cell Biology, Faculty of Medicine, University of Debrecen, Debrecen, Hungary
[5] Immunproteogenomics Extracellular Vesicle Research Group of the Hungarian Academy of Sciences-Semmelweis University, Budapest, Hungary
[6] Extracellular Vesicle Research Group, Hungarian Center of Excellence Molecular Medicine, Budapest, Hungary

This study sought to compare the behavior of Treg subsets displaying different coexpression patterns of Neuropilin-1 (Nrp1) and Helios, under the influence of gut stress unrelated to hematopoietic stem cell transplantation, pretransplantation conditioning, and posttransplant gastrointestinal acute graft versus host disease (GI-aGvHD). Host CD4^{+}/CD25^{hi}/Foxp3^{+} Treg cells, identified by flow cytometry, were isolated from various tissues of mice affected by these stressors. Expression of CD25, CTLA-4, CD39, OX40, integrin-β7, LAG3, TGFβ/LAP, granzyme-A, -B, and interleukin-10 was compared in four Treg subsets displaying Helios or Nrp1 only, both or none. Fluorescence-activated cell sorter–sorted Treg subsets, displaying markers affected in a conditioning- and GI-aGVHD-restricted manner, were further investigated by transcriptome profiling and T-cell suppression assays. We found that conditioning by irradiation greatly diminished the relative frequency of Helios^{+}/Nrp1^{+} Treg, shifting the balance toward Helios^{-}/Nrp1^{-} Treg in the host. Upregulation of integrin-β7 and OX40 occurred in GI-aGvHD-dependent manner in Helios^{+}/Nrp1^{+} cells but not in Helios^{-}/Nrp1^{-} Treg. Sorted Treg subsets, confirmed to overexpress Nrp1, Helios, OX40, or integrin-β7, displayed superior immunosuppressive activity and enrichment in activation-related messenger RNA transcripts. Our data suggest that conditioning-induced shrinkage of the Nrp1^{+}/Helios^{+} Treg subset may contribute to the development of GI-GvHD by impairing gut homing and decreasing the efficiency of Treg-mediated immunosuppression.

Keywords: Acute graft versus host disease · Treg · Neuropilin-1 · CD304 · Helios

Additional supporting information may be found online in the Supporting Information section at the end of the article.

Correspondence: Prof. Zoltán Pós
e-mail: pos.zoltan@semmelweis.hu

Nikolett Lupsa and Barbara Érsek equally contributed.

Introduction

Allogeneic hematopoietic stem cell transplantation (aHSCT) is a potentially curative therapy for various malignant and nonmalignant diseases affecting the hematopoietic system. Upon aHSCT, a side effect of the therapy, acute graft versus host disease (aGvHD) may develop, characterized by high morbidity and mortality [1]. Acute graft versus host disease (GvHD) is a life-threatening complication, the development and intensity of which are associated with the intensity of the pretransplant conditioning regimen. Conditioning causes tissue injury in multiple organs of the host, most notably in the gastrointestinal (GI) tract, and conditioning-mediated gut damage leads to a strong inflammatory reaction supporting extensive priming of graft-derived T cells by host alloantigens. Ultimately, recognition of alloantigens and tissue damage mediated by various graft leukocytes, such as allogeneic $CD8^+$ T cells, paves the way to the development of aGvHD [2]. The main target organs of aGvHD are the skin, the gut, and the liver, and the type and extent of organ involvement greatly affect the prognosis of aGvHD [3, 4]. Nevertheless, it is generally accepted that conditioning-induced gut damage, gut barrier dysfunction, local microbial dysbiosis followed by bacterial invasion, and massive local inflammation are key prerequisites to the development of all organ manifestations of aGvHD [5]. In response to aGvHD, an antiinflammatory host response, characterized by regulatory T-cell (Treg) activation and release of immunosuppressive cytokines, occurs. However, it has been argued that conditioning-related dysfunction of antiinflammatory cells, such as Treg, is instrumental in the subsequent development of aGvHD [6, 7], and it has been shown that in full-fledged disease, Treg are unable to control extensive graft T-cell activation and clonal expansion, leading to widespread tissue damage [5].

Direct experimental analysis of the events leading to the development of human GI-aGvHD, such as the mechanisms responsible for functional Treg failure in affected tissues, is challenging. Collection of biopsies from the inflamed GI tract of aGvHD patients should be minimized, and obtaining gut biopsies for purposes other than diagnostic use is generally contraindicated. As an alternative, analysis of circulating blood $CD4^+$ Tregs is possible, although there are vast differences between GI $CD4^+$ Treg and their circulating counterparts [8]. Finally, animal models may also be utilized, providing access to Treg in affected tissues in situ; however, this approach also has its limitations [9–11].

Regulatory $CD4^+CD25^+Foxp3^+$ T cells play an important role in maintaining immune homeostasis, limiting immune response against self and harmless nonself-antigens, and establishing tolerance [12]. In the early phase of aGvHD, Tregs attempt to hamper the extensive clonal expansion characteristic for allogeneic graft $CD8^+$ T cells, rapid expansion of which is a prerequisite of aGvHD. These features make Treg important prophylactic agents and promising therapeutic targets in the management of patients undergoing aHSCT [13, 14]. However, in full-fledged aGvHD, Treg activity in target organs is critically suppressed by many factors. These include the immunosuppressive conditioning regimen applied before aHSCT, causing variable severity lymphopenia, the abnormal migration of circulating Treg to target tissues, and the inflammatory environment of aGvHD, which affects Treg stability by decreasing FoxP3 expression [15, 16], even allowing the transformation of some Treg subsets into pathological Th cells [17].

Local Treg responses to gut stress, gut damage, and altered Treg functionality in affected GI tissues are not phenomena restricted to aGvHD. Similar findings have been made in several human morbidities affecting the gut, including inflammatory bowel disease (IBD). In IBD, there is general consensus that target tissues are enriched in Tregs [18], and their homeostasis and activity are significantly altered [19, 20]. Recently, while analyzing Treg in an experimental IBD setting, it has been suggested that two markers, Neuropilin-1 (Nrp1, CD304) and Helios, differentially expressed by select GI Treg subsets, relate to extensive, subset-specific differences affecting Treg functionality in IBD [21, 22]. These differences affect the expression of several genes related to Treg functionality, suppressive capacity, and even T-cell receptor for antigen (TCR) specificity in IBD. Nevertheless, it is unknown whether similar differences may be observed between these subsets' behavior in other forms of gut stress, such as pretransplant conditioning, acting as a stressor before aHSCT, or posttransplant GI-aGvHD developed upon aHSCT. Such data may be of particular importance to understand Treg behavior in GI-aGvHD, as heterogeneity in Helios and Nrp1 expression among these cells has been observed both systemically, and in the GI tract from early on [23], but interpretation of these observations turned out to be challenging and underwent substantial changes over time. Initially, Helios and Nrp1 were thought to be appropriate selection markers for distinguishing natural (nTreg) and peripheral (pTreg) subpopulations [24–26] as it was assumed that thymus-derived nTregs exhibit uniformly high Helios and Nrp1 expression compared to pTreg. Later, however, it has become increasingly clear that Treg shows high heterogeneity, and the different levels of Helios and Nrp1 are not exclusive markers of any of the two [13, 27].

Helios is a zinc finger transcription factor (TF) present in about 70% of murine blood circulating Tregs, and Tregs present peripheral lymphoid tissues. In the thymus, more than 95% of Treg cells are $Helios^+$; however, in Helios-deficient mice, thymic Treg development was not affected, which suggests that Helios is not mandatory for thymic Treg lineage commitment [28, 29]. Helios is considered a T-cell activation marker on many T-cell subsets, including, but not limited to, Treg [30, 31], the expression of which is inducible by in vitro TCR activation or TGF-β treatment [25]. Nevertheless, in Treg, it is debated whether Helios represents a factor actively contributing to Treg stability and suppressive function or is merely a marker of activation; finally, species-related differences may exist, as well [32, 33]. Nrp1 is a transmembrane glycoprotein of the semaphorin III receptor [34], playing important roles in the dendritic cell–Treg interaction during antigen presentation. Nrp1 has been described as a factor essential to Treg stability and efficient immunosuppression [35], but it may play other roles as well, as in some solid tumors, it was shown to be involved in the infiltration of the tumor microenvironment by Tregs [36, 37]. Similar to Helios,

originally, Nrp1 was associated with nTreg rather than pTreg cells [34], but later studies and human experiments challenged this view [38]. Nevertheless, the fact that both markers relate to Treg function is clear, and, as mentioned earlier, it is becoming increasingly apparent in GI damage too [21, 22].

The aim of this study was to investigate the behavior of gut-resident, peripheral, and circulating Treg subsets displaying different patterns of Helios and Nrp1 coexpression, under the influence of posttransplant GI-aGvHD (allograft transplantation and GI-aGvHD). Pretransplantation conditioning in the absence of an allograft (syngraft transplantation without GI-aGvHD), and gut stress unrelated to hematopoietic stem cell transplantation (chemically induced IBD).

We demonstrate that, in addition to several similarities observed between the effects of these stressors on host Treg cells, conditioning by irradiation induces unique, characteristic changes in the balance of Treg subsets differentially expressing Nrp1 and Helios. Further, we show that select biomarkers, characteristic for a Treg response in posttransplant GI-aGvHD, appear on host Treg cells in a subset-specific manner, predominantly in the Treg subset most affected by pretransplant conditioning.

Methods

Mice

All animal experiments were conducted with the approval of the Institutional Animal Care and Use Committee and the National Scientific Ethical Committee on Animal Experimentation. All procedures conformed to the Directive 2010/63/EU on the European Convention for the protection of animals used for scientific purposes. Wild-type C57/BL/6J (hereafter B6), B6.SJL-Ptprca Pepcb/BoyJ (B6 CD45.1), C57/BL/6-Tg(CAG-OVA)-916Jen/J (B6 transgenic actin beta promoter-controlled, membrane bound, chicken ovalbumin antigen [Act-mOVA]), C57/BL/6-Tg(TcraTcrb) 1100Mjb/J (B6 OT-I), and B6.Cg-Foxp3tm2(EGFP)Tch/J (B6 Foxp3-green fluorescent protein [GFP]) mice were obtained from The Jackson Laboratory (Bar Harbor, ME, USA). Animals were kept in a minimal disease environment (see Supplementary Data 1), in a temperature-controlled room, in individually ventilated cages, on a 12L:12D cycle, with free access to food and water, with mouse igloos (Tecniplast) providing environmental enrichment. In all experiments, female mice were used at 8–16 weeks of age, treated as described below, or left untreated to serve as internal experimental controls.

B6 and B6 Act-mOVA mice were maintained by breeding wild-type B6 mice to hemyzigote B6 Act-mOVA animals. Cohoused F1 generation littermates were genotyped by quantitative polymerase chain reaction, with Taqman probe sets specific for the chicken ovalbumin (Assay ID: Gg03366807_m1) and mouse transferrin receptor (Assay ID: 4458370) genes, used as test and reference, respectively, to identify B6 and B6 Act-mOVA animals for experiments. Genotyped B6 and B6 Act-mOVA animals were cohoused from birth to the age of 4–6 weeks, thereafter separated, treated, and compared as described below. B6 CD45.1, B6 OT-I, and B6 Foxp3-GFP mice were maintained by homozygous mating, with their genotypes validated by flow cytometry, using CD4-Vioblue, CD45.1-APC (both from Miltenyi Biotec), CD45.2-AlexaFluor700 (BioLegend), CD8-PerCP-Cy5.5 (Transcription Factor Staining Buffer Set [Thermo]), and TCRva2-FITC antibodies (Becton Dickinson). B6 OT-I and B6 Foxp3-GFP mice served as cell donors for experiments, did not receive treatments, and were not compared to other strains.

Allogeneic HSCT

Allogeneic HSCT was performed to induce murine experimental acute GI GvHD as described earlier [39], with modifications implemented to ensure conformity with the European Directive 2010/63/EU by refining protocols to reduce weight loss and host mortality in order to reduce animal suffering and animal numbers used, and in order to minimize the presence of graft Treg in the host by day 4 post-aHSCT. Briefly, B6 act-mOVA mice received 11 Gy total body irradiation (TBI) in two doses, 3 h apart (5.5 Gy each, 137.37 cGy/min). Next, irradiated animals were transplanted with 3×10^6 allogeneic bone marrow cells and 1×10^5 splenocytes obtained from B6 OT-I mice. Recipients were grafted via retroorbital injection, under ketamine–xylazine anesthesia. Pilot experiments were performed to verify the development of GvHD and define optimal timing for Treg isolation; in these experiments, grafted mice were monitored for weight loss, hunchback, ruffled fur, and signs of apathy for 14 days and euthanized on days 4, 7, 9, and 14 after aHSCT by CO_2 asphyxiation. In actual studies, mice were euthanized on day 4 after aHSCT by CO_2 and immediately subjected to tissue removal and processing for downstream analyses.

Syngeneic HSCT

Syngeneic HSCT was performed to induce radiation-mediated experimental gut damage in the context of HSCT without the development of acute GI GvHD. To this end, B6 Act-mOVA mice were used as syngeneic graft donors and their B6 Act-mOVA littermates as graft recipients (B6 Act-mOVA → B6 Act-mOVA). All other conditions of transplantation, graft preparation and transfer, animal monitoring, and tissue removal were performed as described under allogeneic HSCT.

DSS treatment

Administration of dextran sodium sulfate (DSS) solution was used to induce experimental gut damage and colitis in the absence of irradiation-mediated gut damage and acute GI GvHD. In these experiments, 2% DSS (Sigma-Aldrich) was dissolved in drinking water and made available to B6 mice ad libitum, replenished every 2 days. In pilot experiments verifying the development of DSS colitis and defining optimal time points for tissue retrieval, mice were monitored for weight loss, hunched back, diarrhea,

and fecal blood for 7 days and euthanized on days 5–7 by CO_2 asphyxiation. In actual studies, mice were euthanized on day 6 after the beginning of the treatment by CO_2, and tissue samples were collected for downstream analyses.

Tissue sample processing

T cells were isolated from the peripheral blood, spleen, mesenteric lymph nodes (MLNs), small intestinal lamina propria (SILP), small intestinal epithelia (SIEL), large intestinal lamina propria (LILP), and large intestinal epithelia (LIEL) of the analyzed animals, as indicated. Spleen and MLN were disrupted mechanically, using 20 μm strainers. Small and large intestines were processed by automated tissue dissociation using the Mouse Lamina Propria Dissociation kit (Miltenyi Biotec) in a Gentle magnetic-activated cell sorting (MACS) Octo Dissociator with Heating Upgrade (Miltenyi Biotec), followed by Percoll gradient (40%/80%, GE HealthCare) centrifugation, and the isolation of the mononuclear cell fraction for downstream analyses. Erythrocytes were removed using the Pharm Lyse buffer, and T cells were identified and analyzed by flow cytometry or subjected to MACS or fluorescence-activated cell sorter (FACS) sorting for further analyses. In all T-cell isolation procedures, fresh tissue samples were used. Sample processing began within 30 min upon tissue sample retrieval. The median processing time was 40 min for spleen and MLN, 3 h for intestinal samples. Yield was determined by Trypan blue staining, and 0.5×10^6 (median yield for SILP, LILP, SIEL, LIEL, and blood) $- 3 \times 10^6$ cells (spleen, MLN cells) per sample were processed for staining.

Flow cytometry

For flow cytometry, mononuclear cells obtained from tissues were stained with CD4-Vioblue (Miltenyi), CD25-APC (Miltenyi), Foxp3-Vio515 (Miltenyi), Helios PE-Vio615 (Miltenyi), CTLA-4-PE (Miltenyi), OX40-PE (Miltenyi), Nrp1-PerCP-eFluor710 (Thermo), CD39-SuperBright600 (Thermo), LAG3-SuperBright600 (Thermo), TGF-β1/LAP-AlexaFluor594 (R&D), granzyme B (GZMB)-PE-Cy7 (Thermo), granzyme A (GZMA)-PE-Cy7 (Thermo), interleukin-10 (IL-10)-PE-Cy7 (BioLegend), integrin-β7 (ITGB7)-AlexaFluor700 (Novus), CD8-PE-Cy7 (Thermo), and eBioscience Fixable Viability Dye eFluor780 (Thermo) in various combinations, in eight to nine color fluorescent panels (see Supporting Information Table 1), as indicated. Cells were stained using the Foxp3/Transcription Factor Staining Buffer Set (Thermo), following the manufacturer's instructions. Briefly, cells were stained for viability, washed in MACS buffer (Miltenyi), stained for surface antigens, fixed, permeabilized, washed in fix-perm buffer, stained for intracellular antigens, washed, and resuspended in Perm buffer for flow cytometry. Samples were passed through a 20 μm strainer (Miltenyi), and single-cell suspensions were analyzed immediately on a Cytoflex flow cytometer (Beckman Coulter). Marker staining for flow cytometry began immediately upon tissue sample processing; the median processing time was 2.5 h. Raw data were analyzed with FlowJo v.10.8.0 (Becton Dickinson). Markers describing the relative frequency of Treg cells and their subsets were evaluated by comparing percent positivity (CD4, CD25, Foxp3, Nrp1, Helios); the level of expression of Treg markers relating to Treg function was analyzed by comparing mean fluorescence intensity (CTLA-4, OX40, CD39, CD25, LAG3, TGF-β1/LAP, GZMB and A, IL-10, and integrin-beta 7).

FACS sorting

Splenic mononuclear cells were retrieved from the spleens of healthy B6 Act-mOVA/Foxp3-GFP mice, as described under tissue sample processing. Splenocytes were labeled with CD45.1-APC (Miltenyi), CD45.2-AlexaFluor700 (BioLegend), CD4-Vioblue (Miltenyi), CD25-PE (Miltenyi), Nrp1-PerCP-eFluor710 (Thermo), ITGB7-PE (Miltenyi), or OX40-PE (Miltenyi), antibodies, in different panels, as indicated, passed through a 20 μm strainer (Miltenyi), and single-cell suspensions were FACS-sorted using a SH800S sorter (Sony). Purity checks were done upon sorting, by flow cytometry, as shown.

MACS sorting

$CD8^+$ T cells (conventional T cell [Tconv]) were isolated from the spleens of healthy wild-type B6 mice using the $CD8a^+$ T Cell Isolation Kit, mouse (Miltenyi) on an AutoMACS Pro magnetic cell sorter (Miltenyi), using the manufacturer's instructions. Purity of sorted $CD8^+$ T cells was controlled upon sorting, by flow cytometry (not shown).

In vivo cell tracking

For in vivo tracking of graft and host Treg cells after aHSCT, transplantation was performed using CD45.2 B6 OT-I grafts containing CD45.1 B6 Treg cells only, and CD45.2 B6 OVA hosts. To this end, CD45.2 B6 OT-I grafts devoid of Ly/singlet/Live/$CD4^+$/$CD25^{hi}$ Treg cells were prepared by FACS sorting. Next, these samples were spiked with FACS-sorted B6 CD45.1 of Ly/singlet/Live/$CD4^+$/$CD25^{hi}$ Treg cells in numbers equivalent to those of B6 CD45.2 Treg present before depletion. Frequency of CD45.2 B6 OT-I Treg before graft manipulation, successful depletion, purity of CD45.1 B6 Treg used for graft spiking, and frequency of CD45.1 B6 Treg after graft manipulation were assessed by flow cytometry. Finally, the frequencies of graft CD45.1 and host CD45.2 Treg were compared in the peripheral blood, spleen, MLN, SILP, and LILP of transplanted B6 OVA animals on day 4 after aHSCT.

Transcriptome profiling

For transcriptome profiling, Ly/singlet/Live/$CD4^+$/$Foxp3^+$/$Nrp1^+$/$OX40^{bright}$, Ly/singlet/Live/$CD4^+$/$Foxp3^+$/$Nrp1^-$/$OX40^{dim}$,

Ly/singlet/Live/CD4$^+$/Foxp3$^+$/Nrp1$^+$/ITGB7$^+$, and Ly/singlet/Live/CD4$^+$//Foxp3$^+$/Nrp1$^-$/ITGB7$^-$ Treg subsets of Act-mOVA/Foxp3-GFP mice were sorted into the lysis buffer of RNeasy Micro Kit Plus (Qiagen). Ribonucleic acid purity, integrity, and concentration were analyzed on RNA 6000 Pico Chips, with the help of a 2100 Bioanalyzer (both from Agilent). Messenger RNA (mRNA) enrichment, library preparation, and transcriptome profiling by next-generation sequencing (NGS), 6 Gb Pe150, Illumina Hiseq, were done by Novogene Co., Ltd. See the Statistics section for data processing, statistical comparison of the transcriptome data of Treg subsets, and identification of differentially expressed genes (DEGs).

Transcription factor enrichment analysis

TFs involved in the regulation of DEGs were predicted using the CiiiDER algorithm, as described [40]. Briefly, TFs with significant binding site enrichment in DEG promoters were listed using TF databases and dedicated software tools. First, known TF binding sites of the promoters of DEGs in a given statistical comparison were retrieved from the GRCm38.94 assembly using the 2022 core vertebrate nonredundant JASPAR TF database [41] with a deficit limit of 0.15. Next, these sets were compared to a reference set consisting of TF binding sites of unaffected genes in the given comparison (non-DEGs). Non-DEGs were defined as genes with an absolute log2 fold change <0.05 and an average expression above the 25th percentile. Finally, TFs displaying $p < 0.05$ enrichment in the DEG set compared to the non-DEG reference were listed and considered having significant binding site enrichment in the promoters of the given set of DEGs.

In vitro Treg suppression assay

T-cell assays are described in accordance with the MIATA guidelines [42]. For in vitro Treg suppression assays, splenic Ly/singlet/Foxp3$^+$/Nrp1$^+$/OX40^{bright}, Ly/singlet/Foxp3$^+$/Nrp1$^-$/OX40^{dim}, Ly/singlet/Foxp3$^+$/Nrp1$^+$/ITGB7$^+$, and Ly/singlet/Foxp3$^+$/Nrp1$^-$/ITGB7$^-$ Treg subsets of B6 Foxp3-GFP mice were sorted into distinct wells of tissue culture-ready 96-well U-well plates (Sarstedt) in different numbers; that is 12 500, 6250, 3125, and 1563 Treg cell/well each. Treg were sorted directly into 100 μL of Advanced RPMI (Thermo) supplemented with 10% FBS (Thermo), 10 mM HEPES (Thermo), 50 μM β-mercaptoethanol (Sigma-Aldrich), 1% GlutaMAX (Thermo), and 1% penicillin-streptomycin (Thermo). Next, MACS-sorted CD8$^+$ Tconv cells were labeled with a carboxyfluorescein succinimidyl ester (CFSE) tracker (Molecular Probes) and seeded on top of the FACS-sorted Treg cells, 12 500 CD8$^+$ Tconv cells each (1:8, 1:4. 1:2, 1:1 Tconv/Treg ratio) in 50 μL aliquots. Finally, CD8$^+$ Tconv cells were expanded using the Dynabeads Mouse T-Activator CD3/CD28 for T-Cell Expansion and Activation kit (Thermo), that is by aCD3/28 microbeads (cell:bead ratio 1:1) and IL-2 (30 IU/mL). Cell culture volume was adjusted to 250 μL/well; cultures were mixed thoroughly and left undisturbed for 96 h. After 96 h, CD8$^+$ Tconv cells were identified with CD8-PE-Cy7 (Thermo) staining, and the dilution of their carboxyfluorescein succinimidyl ester staining was analyzed by a Cytoflex flow cytometer (Beckman Coulter). For all experiments, monocultures of unstimulated and stimulated CD8$^+$ Tconv cells served as negative and positive controls, respectively. Raw data were analyzed with the cell proliferation module of FlowJo v 10.8.0. Treg-mediated suppression of cell division was calculated based on the cell division index (DI), as follows: percent suppression of clonal expansion = 100 − (DI of Tconv stimulated, left unsuppressed/DI of Tconv stimulated, Treg suppressed) × 100. Sorting parameters, cell culture media, and assay functionality were pretested in pilot studies; percent suppression exceeding 20% was considered proof of Treg-mediated suppression.

In vivo Treg suppression assay

For in vivo Treg co-administration experiments, B6 OVA mice were transplanted either with B6 OT-I grafts as described under allogeneic HSCT or with B6 OT-I grafts containing FACS-sorted Ly/singlet/Foxp3$^+$/Nrp1$^+$/OX40^{bright} or Ly/singlet/Foxp3$^+$/Nrp1$^-$/OX40^{dim} Treg cells. First, Ly/singlet/Foxp3$^+$/Nrp1$^+$/OX40^{bright} and Ly/singlet/Foxp3$^+$/Nrp1$^-$/OX40^{dim} Treg cells of B6 Foxp3-GFP mice were FACS-sorted as described under Treg suppression assays, to U-well plates, 20 000 Treg cells per well. Next, 1×10^5 splenocytes of OT-1 mice were added to sorted Treg subsets (∼2:1 Treg/CD8$^+$ Tconv cell ratio). Finally, B6 OVA mice were grafted with 3×10^6 bone marrow cells and 1×10^5 splenocytes of OT-I mice with or without Treg admixture. Grafted B6 OVA hosts were monitored for weight loss and survival for 12 days after aHSCT.

Statistics

GvHD disease course was analyzed with GraphPad v 9.11 (GraphPad Software, Inc.). Weight loss and survival were analyzed using the mixed effects model and Kaplan–Meier survival analysis, respectively. Results of multiple group comparisons were corrected using the Sidak method; $p < 0.05$ was considered statistically significant.

Flow cytometry data were analyzed in GraphPad to identify Treg markers affected (i) by the applied treatment, (ii) by the local tissue environment, and (iii) by subset (defined by Hrp1 and Helios staining, as indicated), and the interaction of these factors. Treg isolated from the same animal were analyzed in a linked manner, considering the subject/animal as a random factor. Outliers were identified using the Robust regression and Outlier removal method. Paired *t*-tests and one-way, two-way, and three-way analyses of variance (ANOVAs) or repeated measures analysis of variance were used, as appropriate, to identify the impact of factors on Treg marker expression, also analyzing factor interactions. Missing values were handled by using a mixed effects model. Next, Treg markers significantly affected by experimental

factors were introduced into Fisher's least significant difference test as a post hoc test. In all analyses, $p < 0.05$ was considered statistically significant.

For NGS data analysis, FPKM (expected number of fragments per kilobase of transcript sequence per millions base pairs sequenced) was used to estimate gene expression levels [43]. Readcount was normalized with the DESeq method [44], and the negative binomial distribution model was applied to calculate nominal alpha (p-values). Finally, unadjusted p-values were further adjusted for multiple hypothesis testing by the Benjamini–Hochberg method [45] to obtain false discovery rate. Genes displaying log2 fold change ≥ 1 and an adjusted $p < 0.05$ between compared groups were considered differentially expressed (DEGs).

Results

Initial marker screening defines a set of host Treg markers affected by experimental GI-aGvHD across multiple tissue environments

We first sought to identify host Treg markers affected by the rise of severe sublethal acute GI graft versus host disease (GI-aGvHD) developed in the act-mOVA/OT-I antigen-specific transgenic TCR model (Fig. 1A,B). First, we confirmed that the model allows for focused analysis of host Treg on day 4 post-aHSCT (Fig. 1C,D), and next, we sought to define the key factors affecting marker expression (Fig. 2): environs selected to be analyzed, possibly affecting Treg markers were (i) tissue environment, (ii) conditioning-independent gut damage, (iii) conditioning-mediated gut damage, and (iv) allograft-mediated gut damage in aHSCT.

To this end, a comprehensive marker screening of host Treg cells was performed by multiparametric flow cytometry in the peripheral blood, spleen, MLN, SILP, LILP, and among the small and large intestinal intraepithelial lymphocytes (SIEL, LIEL, respectively) of mice developing gut damage induced in a conditioning/HSCT-independent manner (DSS colitis), upon conditioning (syngeneic HSCT), and in GI-aGVHD (allogeneic HSCT). Tregs retrieved from the above tissues were identified as Ly/Live/CD4$^+$/CD25$^+$/Foxp3$^+$ cells [46–48] and tested for the expression of CD25, OX40 (CD134), Helios, Nrp1, CD39, LAG3, CTLA-4, LAP/TGF-β1, IL-10, ITGB7, GZMB, and GZMA; see Fig. 2A for Treg gating strategy and representative results obtained by flow cytometry.

We first categorized Treg markers to identify markers affected either by the most relevant stressor, that is GI-aGvHD following aHSCT, and the relevance of tissue environment, as a possible cofactor affecting Treg marker behavior. We ordered subset-specific and functionality-related Treg markers into three categories, that is we identified markers affected by GI-aGvHD following aHSCT (Fig. 2B), by tissue localization (Fig. 2C), or by GI-aGvHD depending on tissue localization (Fig. 2D). As expected, aHSCT and the rise of GI-aGvHD had a profound effect on Treg numbers in GvHD target organs (see Supporting Information Fig. 1). In addition to Treg depletion, aHSCT followed by GvHD clearly affected host Treg subset frequency (Fig. 2E) and marker expression (Fig. 2F), too, by decreasing the frequency of Treg subsets expressing Helios ($p < 0.0001$) and Nrp1 ($p < 0.0001$), decreasing surface levels of CD25 ($p = 0.0002$) on Treg, and elevating the levels of LAG3 ($p = 0.0278$), LAP/TGFβ1 (LAP/TGFb, $p = 0.0057$), ITGB7 ($p = 0.0129$), and OX40 ($p = 0.0009$) (Fig. 2E,F). Tissue localization altered the expression of CD39 on host Treg ($p < 0.0001$), although CD39 remained completely unaffected by GI-aGvHD itself (Fig. 2C). On the other hand, we also found that the effect of GI-aGvHD was dependent on tissue environment in case of LAG3 ($p = 0.0053$) and LAP/TGF-β1 ($p = 0.002$) (Fig. 2D) as they were induced by GI-aGvHD in Tregs present in SLOs (spleen and MLN) but remained unaffected within the target organs of the disease (LILP and SILP). Treg cells' staining for GZMA, GZMB, IL-10, and CTLA-4 remained unaffected by both tissue localization and GI-aGvHD (not shown). At the end of the initial marker screening, all Treg markers unaffected by GI-aGvHD, and unaffected by GvHD in target tissues, that is CD39, CTLA-4, LAG3, LAP/TGFb1, GZMA, GZMB, and IL-10, were excluded from further studies. Moreover, as under no circumstances analyzed was the presence or immigration of Treg in the IEL compartments observed during the rise of aGvHD (Supporting Information Fig. 1), these tissues were also removed from further analysis.

Conditioning by irradiation induces unique, characteristic shrinkage of the host Nrp1$^+$/Helios$^+$ Treg subset before the development of GI-aGvHD

Considering that the presence or absence of Helios and Nrp1 in Treg cells was shown to deeply affect Treg functionality in GI tissue damage caused by IBD [21, 22], and that no such data are available in gut damage caused by conditioning or GI-aGVHD, we next set out to clarify the relationship between the behavior of these markers and IBD-linked gut damage, conditioning-induced gut damage, and GI GvHD. To this end, we tested their expression in gut damage unrelated to both irradiation and GI-aGvHD (IBD developed in DSS colitis), irradiation-induced gut damage without GI-aGvHD (syngraft transplantation), and irradiation-induced gut damage with GI-aGvHD (allograft transplantation). Our analysis disclosed that some Treg markers, such as CD25, were affected by all analyzed forms of gut stress evaluated, in virtually the same manner, and hence, these changes may bear limited specific relevance to GI-aGvHD (Fig. 3A). In contrast, a markedly decreased frequency of Nrp1- and Helios-positive Treg was significantly associated with pretransplant conditioning (syngraft transplantation) and posttransplant GI-aGVHD (allograft transplantation) (Fig. 3A). Considering that in aHSCT, pretransplant conditioning predates the posttransplant rise of GI-aGvHD, that the former is a prerequisite of the latter, and that there was virtually no difference between the effect of these two stressors on the frequency of Nrp1$^+$ and Helios$^+$ Treg,

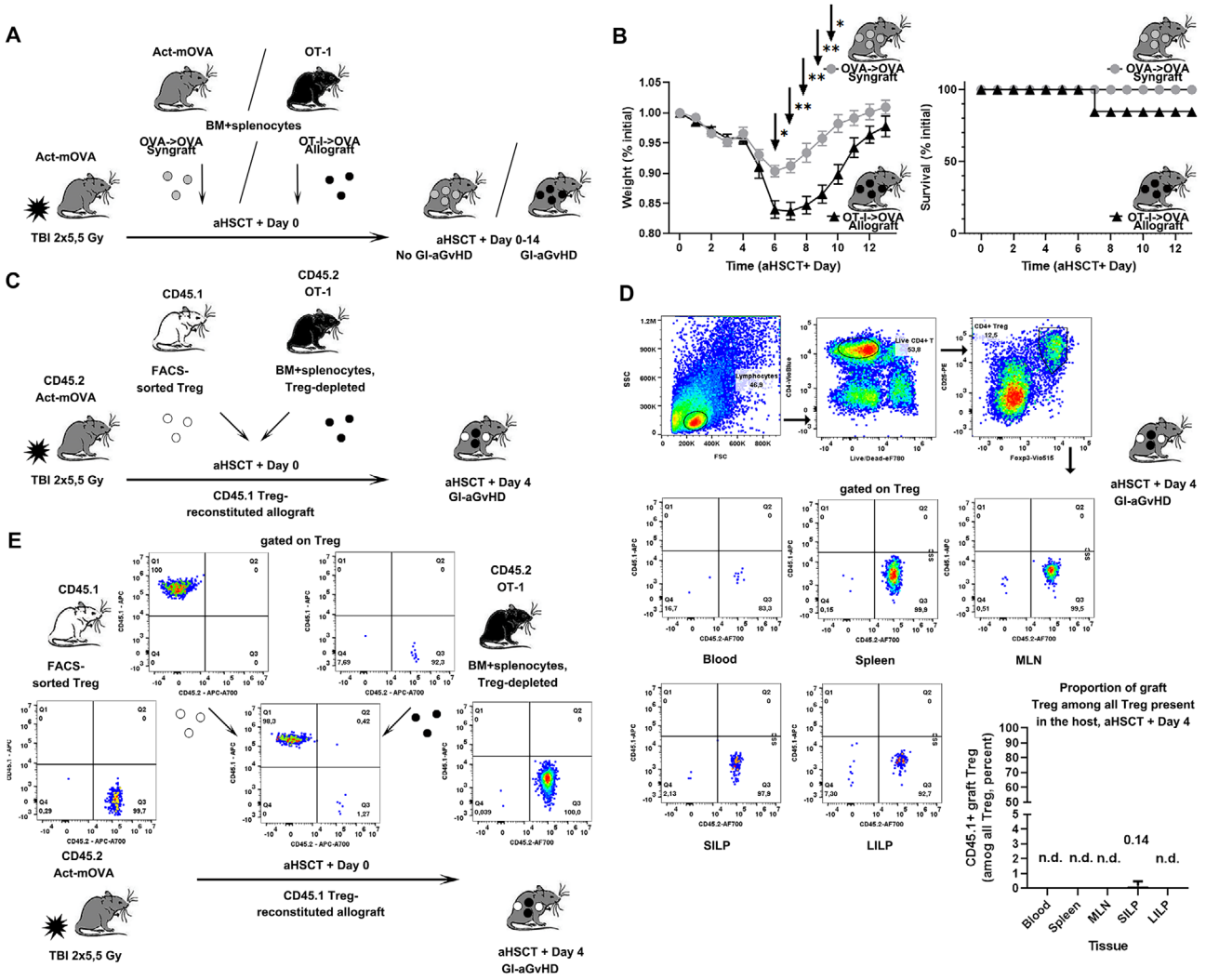

Figure 1. Experimental setup and model validation: the OT-I/transgenic actin beta promoter-controlled, membrane-bound, chicken ovalbumin antigen (Act-mOVA) antigen-specific transgenic T-cell receptor for antigen (TCR) model of gastrointestinal acute graft versus host disease (GI-aGvHD) in the analysis of host Treg cells, day 4 post-allogeneic hematopoietic stem cell transplantation (aHSCT). (Panel A) Allograft-induced sublethal GI-aGvHD developed in a transgenic TCR-based (OT-I), minor allele mismatch (OVA) murine model of GI-aGvHD, as compared to lethal dose total body irradiation (TBI) rescued by syngraft administration. (Panel B) Weight loss and host survival in GI-aGvHD following allogeneic HSCT, as compared to syngeneic HSCT serving as reference. The weight loss graph displays daily changes in body weight of the experimental groups indicated, mean and SEM, compared to initial (percent). The Kaplan–Meier plot shows overall survival in the same groups (percent). Black: GI-aGvHD induced in B6 Act-mOVA mice after conditioning by lethal dose TBI and allograft transfer using B6 OT-I mice as graft donors (OT-I → OVA allograft/GI-aGvHD) Gray: syngeneic HSCT using the same conditioning regimen, but syngraft transfer performed with B6 OVA mice serving as graft donors (OVA → OVA syngraft/no GI-aGvHD). Summary of two independent experiments, $n = 7$ each, $n = 14$ total, mixed model analysis of variance (ANOVA), arrows and stars indicate significant differences in the Sidak test; $^{*}p < 0.05$, $^{**}p < 0.01$. (Panel C) In vivo tracking of CD45.1^{+} graft-derived, and CD45.2^{+} host Treg cells in different tissues of a CD45.2^{+} B6 OVA host 4 days after B6 OT-I allograft transplantation. (Panel D) relative frequencies of CD45.1^{+} graft- and CD45.2^{+} host-derived Treg in the blood, spleen, mesenteric lymph nodes (MLN), small intestinal lamina propria (SILP), and large intestinal lamina propria (LILP) of the host on day 4 post-allogeneic hematopoietic stem cell transplantation (aHSCT) (representative data and results of one experiment are shown, $n = 4$; the bar graph displays mean and SD). (Panel E) Validation of the fluorescence-activated cell sorter (FACS)-assisted replacement of graft CD45.2 Treg with equal numbers of CD45.1 Treg. Representative data showing CD45.1 and CD45.1 stainings of cells within the Treg gate after FACS-assisted CD45.2^{+} Treg depletion, CD45.1^{+} Treg sorting, and CD45.1^{+} Treg reconstitution of the graft.

the data suggest that Helios and Nrp1 were affected by conditioning, present in both experimental groups, and this effect propagated to subsequent GI-aGvHD (Fig. 3A). Further analysis made it clear that pretransplant conditioning shifted the subset distribution of host Treg cells in a selective, subset-dependent manner. Conditioning strongly diminished the relative frequency of Nrp1^{+}/Helios^{+} Treg cells within the Treg compartment, whereas it elevated that of their Nrp1^{-}/Helios^{-} counterparts (Figs. 3B and 4). In contrast, the relative frequency of single positive, that is Nrp1^{-}/Helios^{+} or Nrp1^{+}/Helios^{-} Treg, remained less affected, if at all, by the analyzed stressors (Fig. 4). Of note, this effect occurred widespread, in

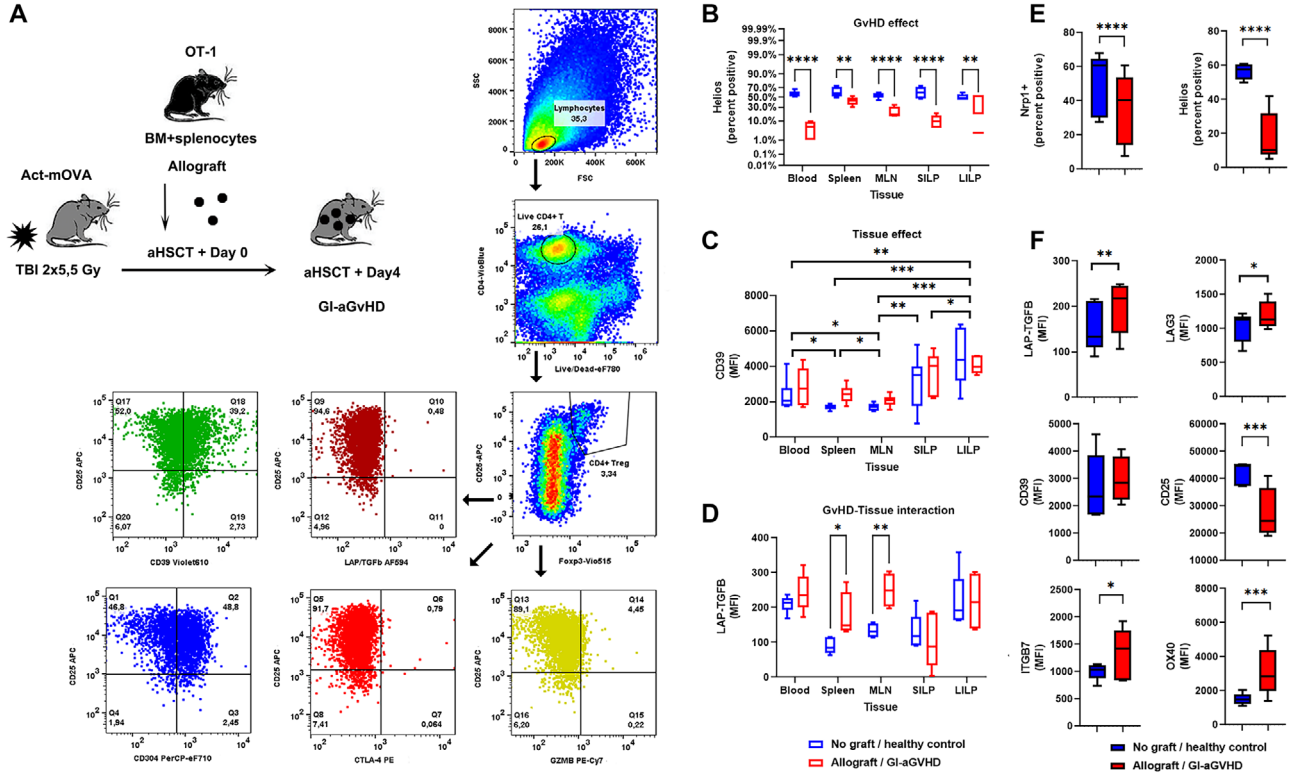

Figure 2. Initial marker screening: Identification of Treg markers affected by the development of gastrointestinal acute graft versus host disease (GI-aGvHD), by local tissue environment, and by GI-aGvHD in a tissue-dependent manner. (Panel A) Flow cytometric gating strategy defining Treg cells of a murine host developing GI-aGvHD in the OT-I/transgenic actin beta promoter-controlled, membrane-bound, chicken ovalbumin antigen (Act-mOVA) model of sublethal GI-aGvHD. Representative data obtained from a nine-color flow cytometric Treg marker panel showing staining of splenic Treg for CD25 versus. Neuropilin-1 (Nrp1), CTLA-4, granzyme B (GZMB), CD39, and LAP/TGFβ. (Panels B–D) Representative examples of (B) Treg markers affected by GI-aGvHD regardless of the tissue environment (e.g. Helios), (C) Treg markers affected by local tissue environment irrespective of the presence and absence of GI-aGVHD (e.g. CD39), and (D) Treg markers affected by GI-aGvHD in a tissue-restricted manner (e.g. LAP/TGFb). Marker staining in the blood, spleen, mesenteric lymph nodes (MLN), small intestinal lamina propria (SILP), and large intestinal lamina propria (LILP) is shown, as assessed by flow cytometry. Untreated healthy controls (blue) are compared to mice with GI-aGvHD (red). Stars indicate significant differences observed in three different statistical comparisons, as indicated above each diagram. Box and whisker plots display results of two independent experiments, $n = 3$ each, $n = 6$ total, min, max, and median values, with groups compared with two-way analysis of variance (ANOVA); results of Fisher's least significant difference (LSD) test are shown by stars; $^{*}p < 0.05$, $^{**}p < 0.01$, $^{***}p < 0.001$, $^{****}p < 0.0001$. (Panels E and F) Summarized data of all identified host Treg subsets (E) and markers (F) that were affected by GI-aGvHD across multiple tissue environments (blood, spleen, MLN, LILP, SILP); untreated healthy controls (blue) are compared to mice with GI-aGvHD (red). Box and whisker plots display results of two independent experiments, $n = 3$ each, $n = 6$ total, min, max, and median values, groups compared with a two-way ANOVA; the significance of GI-aGvHD as a factor is shown by stars; $^{*}p < 0.05$, $^{**}p < 0.01$, $^{***}p < 0.001$, $^{****}p < 0.0001$.

virtually all tissues analyzed (Fig. 4). Taken together, a reduction of the relative frequency of Nrp1^{+}/Helios^{+} Treg, accompanied by an increase in the relative frequency of Nrp1^{-}/Helios^{-} Treg, were phenomena characteristic for a host developing GI-aGvHD, but they were conditioning-induced events, not directly related to aGvHD, and they occurred as systemic changes affecting multiple tissues of the host.

Acute gastrointestinal GvHD increases expression of OX40 and ITGB7 on Treg cells, unlike conditioning by irradiation or conditioning-independent gut damage

Next, we sought to identify Treg markers differentially regulated by Nrp1^{+}/Helios^{+} and Nrp1^{-}/Helios^{-} Treg, which were closely linked to the development of GI-aGvHD, but not the other two analyzed stressors, that is irradiation-dependent and -independent gut barrier damage. Among the markers analyzed, OX40 and ITGB7 fulfilled these latter criteria. OX40 and ITGB7 showed significantly increased expression in allografted animals developing GI-aGvHD compared to healthy controls, and this behavior differed significantly from their reaction or their lack of reaction to either radiation-dependent or -independent gut damage (Fig. 5A).

The Nrp1^{+}/Helios^{+} Treg population is the subset most prone to express gut homing and activation markers in posttransplant GI-aGvHD

We next sought to clarify if there was any difference between the Treg subsets most affected by pretransplant conditioning in terms of their relative contribution to the increased ITGB7 and OX40

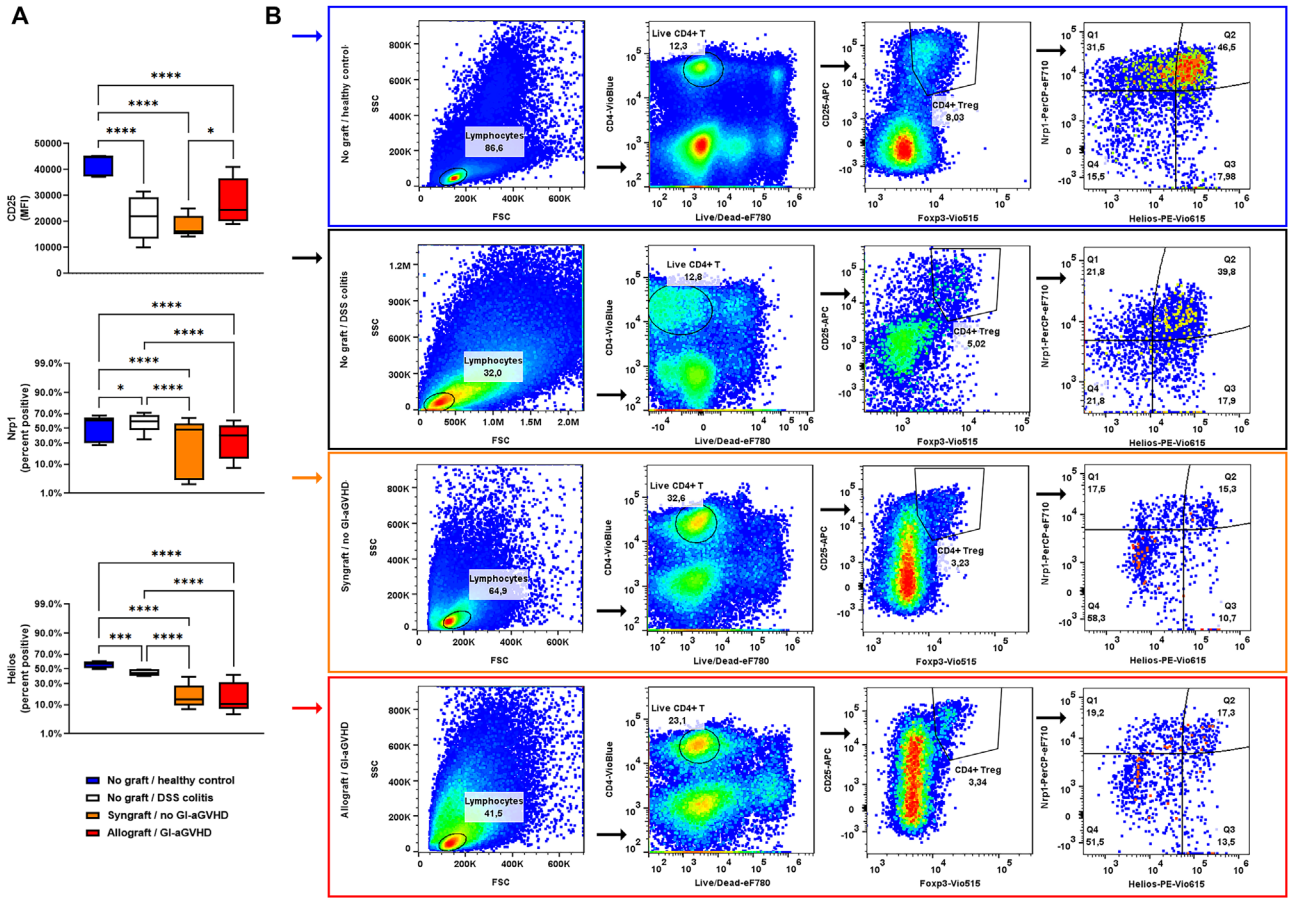

Figure 3. Similar changes in host Treg CD25 expression and the relative frequency of Neuropilin-1 (Nrp1)$^+$ and Helios$^+$ Treg subsets in three distinct forms of gut damage: dextran sodium sulfate (DSS) colitis, total body irradiation, and gastrointestinal acute graft versus host disease (GI-aGvHD). (Panel A) Alterations in host Treg cells' CD25 expression and Treg subset frequencies displaying Nrp1 and Helios in three distinct forms of gastrointestinal stress. Summarized data obtained from the blood, spleen, mesenteric lymph nodes (MLN), small intestinal lamina propria (SILP), and large intestinal lamina propria (LILP) of untreated healthy control mice (blue), mice with DSS-induced gut damage (white), mice undergoing conditioning by irradiation without the development of GI-aGvHD (orange), and animals with conditioning and GI-aGvHD (red). Box and whisker plots show results of two independent experiments, $n = 3$ each, $n = 6$ total, min, max, and median values. Data analyzed by two-way analysis of variance (ANOVA), stars indicate results of Fisher's least significant difference (LSD) test; $^*p < 0.05$, $^{***}p < 0.001$, $^{****}p < 0.0001$. (Panel B) Representative raw data showing typical patterns of CD25, Nrp1, and Helios staining in splenic Tregs; frames indicate treatment groups by color (blue, white, orange, and red).

expression in posttransplant GI-aGVHD. Flow cytometric staining patterns suggested that Helios$^+$ and Nrp1$^+$ Treg may express higher levels of OX40 and ITGB7, than their Helios$^-$ and Nrp1$^-$ counterparts, and this difference remained stable both in the presence and absence of GI-aGvHD (see Fig. 5B for representative flow data). Statistical analysis of Treg obtained from all analyzed tissues confirmed this (Fig. 5C); the presence of Helios in Treg cells was associated with higher levels of both ITGB7 ($p < 0.0001$) and OX40 ($p < 0.0001$) expressions, and a similar link could be established between the presence of Nrp1 and both ITGB7 ($p = 0.0115$) and OX40 ($p = 0.0080$), too.

Further statistical analysis revealed that these differences may be markedly affected by GI-aGvHD, in a marker- and tissue environment–dependent manner (Fig. 6). We found that in GI-aGvHD, only Helios$^+$ Treg react with a further extension of the already elevated expression of ITGB7 (interaction between GvHD and Helios status as factors $p < 0.001$), whereas such a reaction was virtually absent in Helios$^-$ Treg, and this difference was apparent in all analyzed tissues (Fig. 6A top). A similar, albeit weaker link (tissue as additional modifier effect, $p = 0.0171$) was found between Helios$^+$ status and the readiness to further upregulate OX40 (Fig. 6A bottom). In contrast, Nrp1$^+$ status was less influential to the reactivity in GvHD; Nrp1$^+$ Treg displayed higher levels of OX40 in secondary lymph organs and the SILP of animals affected by GI-aGvHD (Fig. 6B bottom), but the presence of Nrp1 did not affect their readiness to upregulate ITGB7 (Fig. 6B top). Taken together, these data suggest that pretransplant conditioning decreases the relative size of those Treg subsets among Treg cells, displaying Helios and Nrp1, which have the high potential to upregulate two, activation- and gut homing–related markers (OX40 and ITGB7) in many tissues affected by posttransplant GI-aGvHD. In contrast, conditioning by irradiation favors Helios$^-$/Nrp1$^-$ Treg, which are not capable of responding to GI-aGVHD.

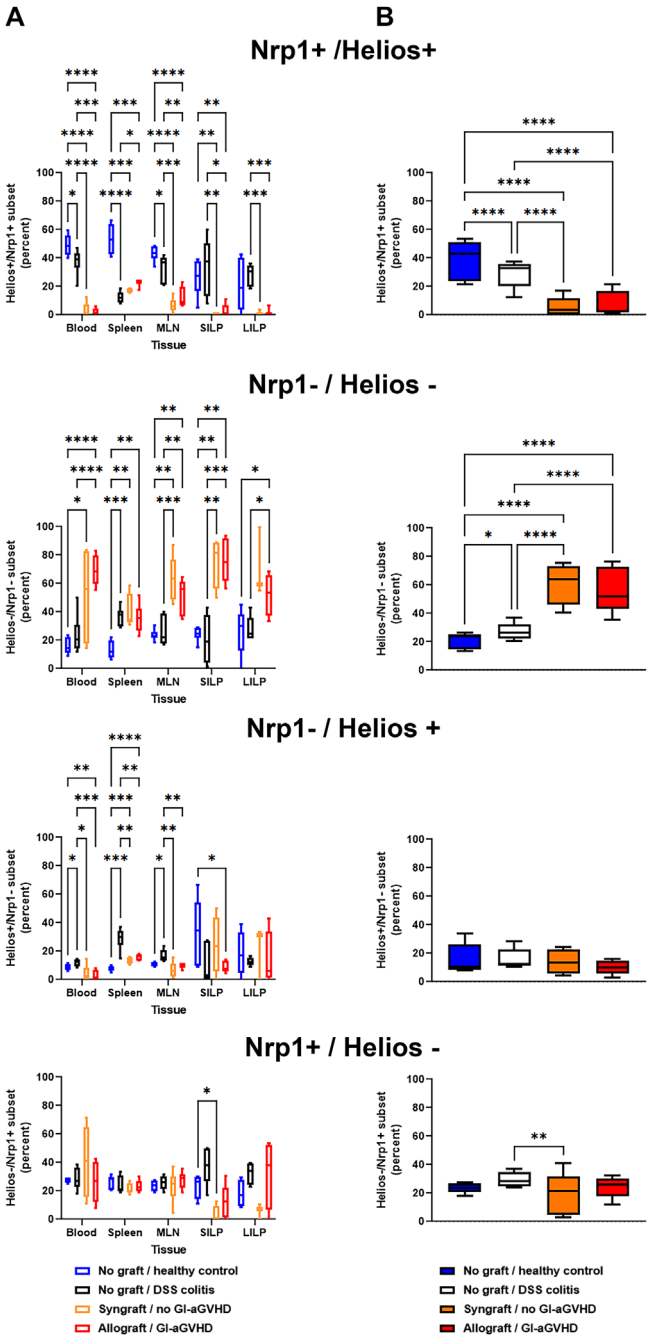

Figure 4. Pretransplant conditioning induces marked shrinkage of the host Neuropilin-1 (Nrp1)$^+$/Helios$^+$ Treg subset; an effect propagated to posttransplant gastrointestinal acute graft versus host disease (GI-aGvHD). Relative frequency of four Treg subsets, defined as Nrp1$^+$/Helios$^-$, Nrp1$^+$/Helios$^+$, Nrp1$^-$/Helios$^+$, and Nrp1$^-$/Helios$^-$ Treg cells, shown in various tissues, as affected by different forms of gut damage. Panel (A) displays respective subset frequencies in the peripheral blood, spleen, mesenteric lymph nodes (MLN), SIPL, and large intestinal lamina propria (LILP), comparing animals in health (blue), in dextran sodium sulfate (DSS)-induced GI damage (white), in conditioning without GI-aGvHD (orange), and in conditioning followed by the development of full-fledged GI-aGvHD (red). Box and whisker plots summarize results of two independent experiments, $n = 3$ each, $n = 6$ total, min, max, and median values. Two-way analysis of variance (ANOVA), stars indicate results of Fisher's least significant difference (LSD) test; $^*p < 0.05$, $^{***}p < 0.001$, $^{****}p < 0.0001$. Panel (B) displays summarized data showing the four subsets affected by treatment only, across all analyzed tissues; blood, spleen, MLN, SIPL, and LILP. Box and whisker plots show results of two independent experiments, $n = 3$ each, $n = 6$ total, min, max, and median. One-way ANOVA; stars indicate results of Fisher's LSD tests; $^*p < 0.05$, $^{**}p < 0.01$, $^{***}p < 0.001$, $^{****}p < 0.0001$.

Transcriptome profiling confirms that host Treg subsets sensitive to conditioning by irradiation are related but functionally divergent and display activated, gut-homing phenotypes

To better understand functional consequences of conditioning-mediated shrinkage of Treg subsets in a healthy host undergoing aHSCT, we further analyzed these subsets by transcription profiling and live Treg suppression assays. Considering that permeabilization for Helios staining is not compatible with live Treg sorting and hence live Treg suppression assays, we opted for two different, Helios-independent sorting strategies to compare the Treg subsets most affected by conditioning and GI-aGvHD.

First, we sorted splenic Ly/singlet/live/CD4$^+$/Foxp3$^+$/Nrp1$^+$/OX40^{bright} Treg to be compared with their Ly/singlet/live/CD4$^+$/Foxp3$^+$/Nrp1$^-$/OX40^{dim} Treg counterparts. Next, we sorted Ly/singlet/live/CD4$^+$/Foxp3$^+$/Nrp1$^+$/ITGB7$^+$ Tregs to be analyzed in comparison with Ly/singlet/live/CD4$^+$/Foxp3$^+$/Nrp1$^-$/ITGB7$^-$ Tregs (Fig. 7A,B). Purity of the sorted Treg subsets was verified by flow cytometry (Fig. 7C). NGS confirmed that the sorted subsets expressed Nrp1 ($p < 0.0001$), OX40 mRNA ($p < 0.0001$), and Helios ($p < 0.0001$) at different levels, in line with surface staining, and expectations based on the close linkage observed between them (Fig. 7D). Mean ITGB7 mRNA levels followed the staining pattern, but this difference did not reach significance after multiple testing corrections ($p = 0.094$, Fig. 7D).

Principal component analysis confirmed that individual samples obtained from the four sorted Treg subsets clustered closely together (Fig. 7E), suggesting the existence of important between-subset differences in their global gene expression patterns. Further, both principal component analysis and multiple testing-corrected pairwise statistics disclosed higher variation between Treg subsets sorted for Nrp1 and OX40 than for Nrp1 and ITGB7 (Fig. 7E). Functional analysis of genes differentially expressed (DEGs) by the four Treg subsets (Fig. 8A), performed with the help of the GO Ontology, KEGG, and Reactome pathway databases, revealed several differences and overlaps in the gene sets expressed by Treg displaying these markers either individually, or in combination. Nrp1/OX40 coexpression affected gene sets most enriched in transcripts related to cytokine signaling and Treg activation, that is costimulatory ligands (upregulated OX40L, LIGHT) egress from secondary lymphoid organs into tissues (e.g. downregulated CCR7), markers characteristic or required for the maintenance of a stable Treg phenotype, Treg survival, Treg expansion (GITR, IL7, TNFRSF15), and increased suppressive potential (upregulated IL-10, CCR8, IL1R2, IL33). Nevertheless, several signatures of enhanced inflammatory cytokine production were also observed, as well, possibly hinting to the complex nature of OX40 signaling in Treg, and its context-dependent

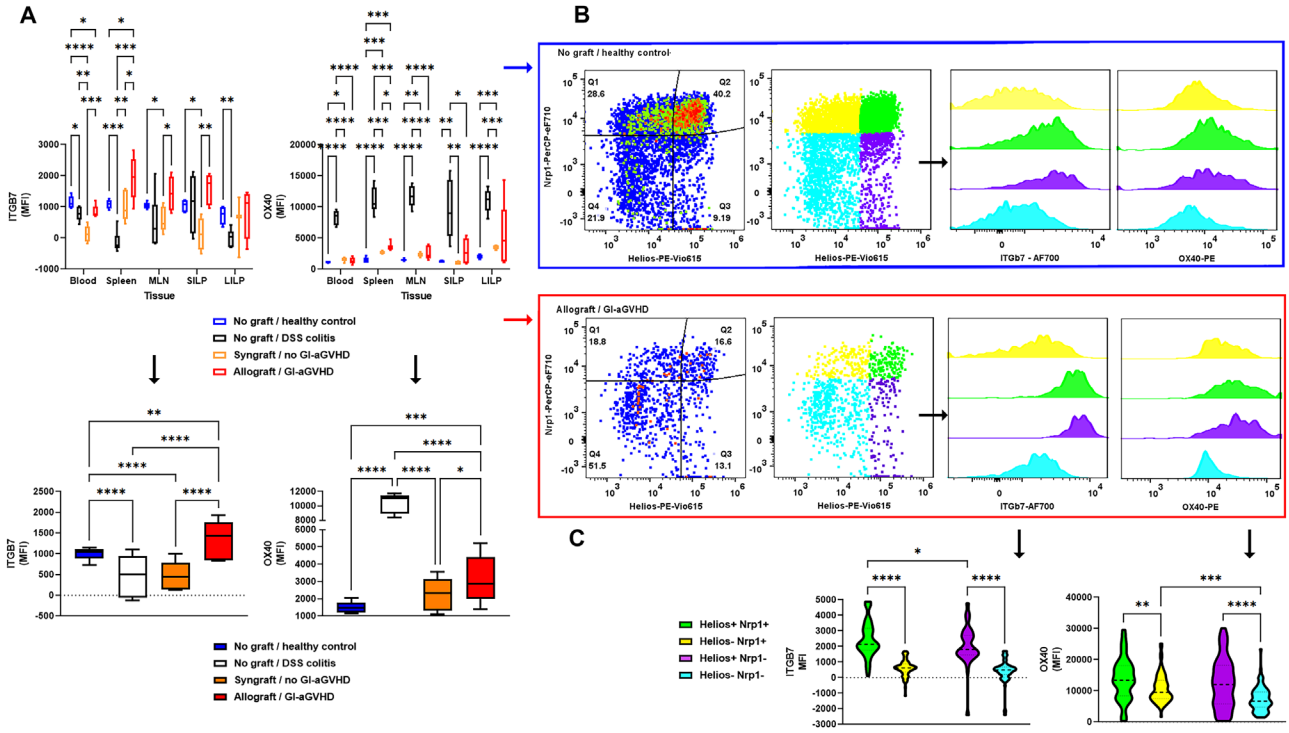

Figure 5. Gastrointestinal acute graft versus host disease (GI-aGvHD) affects Treg cells' integrin-β7 (ITGB7) and OX40 expressions, unlike other stressors of the GI tract. (Panel A) Changes in the host Treg cells' ITGB7 and OX40 expressions in GI-aGvHD, as compared to other stressors. ITGB7 and OX40 stainings of host Treg cells in health, in distinct forms of gut damage without GvHD, and in GI-aGvHD. Top: data obtained from the blood, spleen, mesenteric lymph nodes (MLN), SIPL, and large intestinal lamina propria (LILP) of healthy control animals (blue), of mice affected by dextran sodium sulfate (DSS)–induced gut damage (white), and of conditioned mice without and with GI-aGvHD (orange and red, respectively). Box and whisker plots show results of two independent experiments, $n = 3$ each, $n = 6$ total, min, max, and median, analyzed with two-way analysis of variance (ANOVA); stars indicate results of Fisher's least significant difference (LSD) test; $^{*}p < 0.05$, $^{**}p < 0.01$, $^{***}p < 0.001$, $^{****}p < 0.0001$. Bottom: summarized data depicting treatment-dependent changes across all tissues analyzed; blood, spleen, MLN, SIPL, and LILP. Box and whisker plots with results of two independent experiments, $n = 3$ each, $n = 6$ total, min, max, and median, analyzed with two-way ANOVA, stars indicate results of Fisher's LSD test; $^{*}p < 0.05$, $^{**}p < 0.01$, $^{***}p < 0.001$, $^{****}p < 0.0001$. (Panels B and C) Linking Treg subsets targeted by pretransplant conditioning to markers affected by posttransplant GI-aGvHD. Dissection of the host Treg heterogeneity along Neuropilin-1 (Nrp1) and Helios, with focus on ITGB7 and OX40 expressions. Representative data showing splenic Treg in health (blue frame) and in GI-aGvHD (red frame) and statistical analysis comparing ITGB7 (left) and OX40 (right) levels in Treg depending on the presence and absence of Helios and Nrp1 coexpressions. Violin plots display, results of two independent experiments, $n = 3$ each, $n = 6$ total, min-to-max data distribution, analyzed by two-way ANOVA. Stars indicate results of Fisher's LSD test; $^{*}p < 0.05$, $^{**}p < 0.01$, $^{***}p < 0.001$, $^{****}p < 0.0001$.

potential to destabilize Treg, and interfere with their suppressive function (Fig. 8B). It was apparent that these genes show a significant overlap with others' reports on the transcriptional profile linked to Helios positive Treg [21], suggesting that subsets compared by NGS indeed strongly differ in their Helios expression.

In contrast, the Nrp1/ITGB7 status affected a smaller set of mRNA transcripts in Treg cells, without significant enrichment in any known functional gene network or functional cluster of transcripts. Nevertheless, several adhesion- and cytoskeleton-related Treg genes were found to be upregulated in Nrp1-/ITGB7-positive Treg, which is consistent with their expected linkage to movement and cell adhesion, both being important components of tissue-specific homing (Fig. 8C).

Finally, NGS transcriptome profiling identified several mRNA transcripts, related to Treg cells' functional maturation, increased suppressive activity, or increased sensitivity to external signals enhancing Treg-mediated suppression [49–55], which were enriched in both Ly/singlet/Foxp3^{+}/Nrp1^{+}/OX40^{bright} Treg and Ly/singlet/Foxp3^{+}/Nrp1^{+}/ITGB7^{+} Treg, as compared to their Ly/singlet/Foxp3^{+}/Nrp1^{-}/OX40^{dim}, and Ly/singlet/Foxp3^{+}/Nrp1^{-}/ITGB7^{-} counterparts, respectively (Fig. 8D).

To further elucidate the mechanistic background of these observations and better understand the transcriptional control of the DEGs in the analyzed four Treg subsets, we performed TF binding site enrichment analysis using CiiiDER [40]. We found that binding sites of several TFs known to be involved in Treg activation and function, such as IRF4, NFKB, BACH2, EOMES, AP-1, STAT5, MYB, BATF, and RUNX1 [56, 57], are significantly enriched in the promoters of affected genes, suggesting their active involvement in shaping the phenotype of the subsets analyzed (Fig. 8E). However, it was also apparent that Treg Nrp1/OX40 status was linked to a far larger number of Treg-relevant TFs than the presence or absence of Nrp1/ITGB7 (Fig. 8E), supporting the notion that Nrp1/OX40 affects multiple aspects of Treg function, whereas Nrp1/ITGB7 influences a rather limited set of Treg-relevant genes.

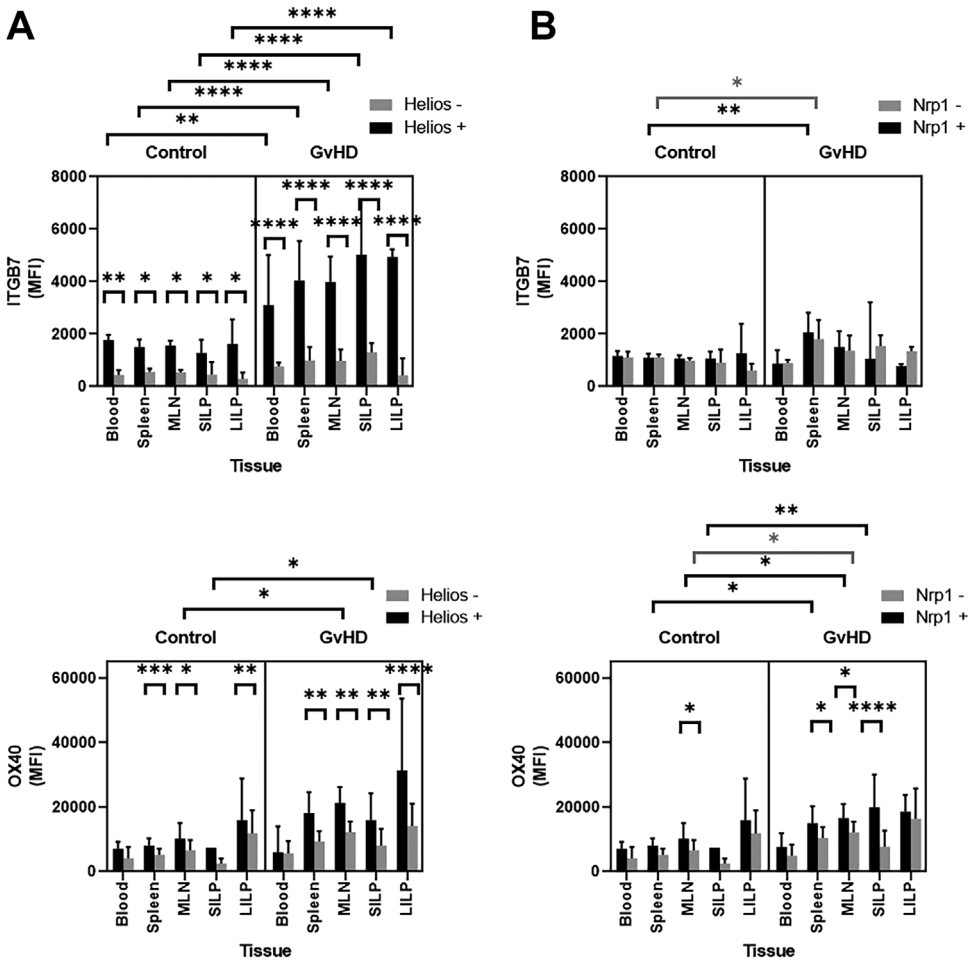

Figure 6. Treg subsets highly sensitive to pretransplant conditioning show stronger commitment to gut-homing and display increased responsiveness in gastrointestinal acute graft versus host disease (GI-aGvHD). Differences in the response of host Treg subsets displaying or lacking Helios (A) and Neuropilin-1 (Nrp1) (B) to the development of GI-aGvHD. Expression of integrin-β7 (ITGB7) (top) and OX40 (bottom) are shown. (Panel A) Responsiveness of Helios$^+$ Treg (black) to GI-aGvHD, as compared to that of Helios$^-$ Treg (gray), assessed by their readiness to upregulate markers of gut homing (ITGB7) and activation (OX40). Bar graphs display results of two independent experiments, $n = 3$ each, $n = 6$ total, mean and SD, evaluated by three-way analysis of variance (ANOVA); results of Fisher's least significant difference (LSD) test are shown by stars; $^*p < 0.05$, $^{**}p < 0.01$, $^{***}p < 0.001$, $^{****}p < 0.0001$. In-frame bars and stars indicate significant differences observed between Helios$^+$ and Helios$^-$ Treg subsets, in the same tissue, under the same conditions. Above-frame bars and stars display differences in the marker expression of a given Treg subset, in a given tissue, between health and GI-aGvHD. Above-frame bars and stars are color-coded; black = Helios$^+$ Treg, gray = Helios$^-$ Treg (none found). (Panel B) Similar analysis of the impact of the presence and absence of Nrp1 on ITGB7 and OX40 expressions displayed by Treg in health and GI-aGvHD. Bar graphs display results of two independent experiments, $n = 3$ each, $n = 6$ total, mean, and SD, analyzed by three-way ANOVA; results of Fisher's LSD test are shown by stars; $^*p < 0.05$, $^{**}p < 0.01$.

CD4$^+$ Treg subsets displaying high sensitivity to conditioning by irradiation exert tighter control over CD8$^+$ T-cell expansion

Finally, we compared the functional properties, and the live suppressive capacity of the Treg subsets most affected by conditioning and GI-aGvHD. To this end, we introduced the above four Treg subsets into standard suppression assays and assessed their capacity to inhibit clonal expansion of cocultured CD8$^+$ T cells upon aCD3/28 stimulation.

We found that host Treg subsets prone to shrinkage upon pretransplant conditioning and displaying makers characteristic for Treg reactive to GI-aGVHD were more capable suppressors of Tconv expansion than those Treg subsets that were not affected by these stressors. Statistical analysis confirmed that Ly/singlet/Foxp3$^+$/Nrp1$^+$/OX40^{bright} Treg were more immunosuppressive in standard suppression assays than Ly/singlet/Foxp3$^+$/Nrp1$^-$/OX40^{dim} Treg cells ($p = 0.0003$, Fig. 8F). Similarly, Ly/singlet/Foxp3$^+$/Nrp1$^+$/ITGB7$^+$ Treg suppressed division of Tconv cells more efficiently than their Ly/singlet/Foxp3$^+$/Nrp1$^-$/ITGB7$^-$ counterparts ($p < 0.0001$, Fig. 8F).

Taken together, results obtained by NGS transcriptome profiling and Treg suppression assays suggested that Treg subsets most affected by pretransplant conditioning, and posttransplant GI-aGvHD belong to functionally different but related Treg

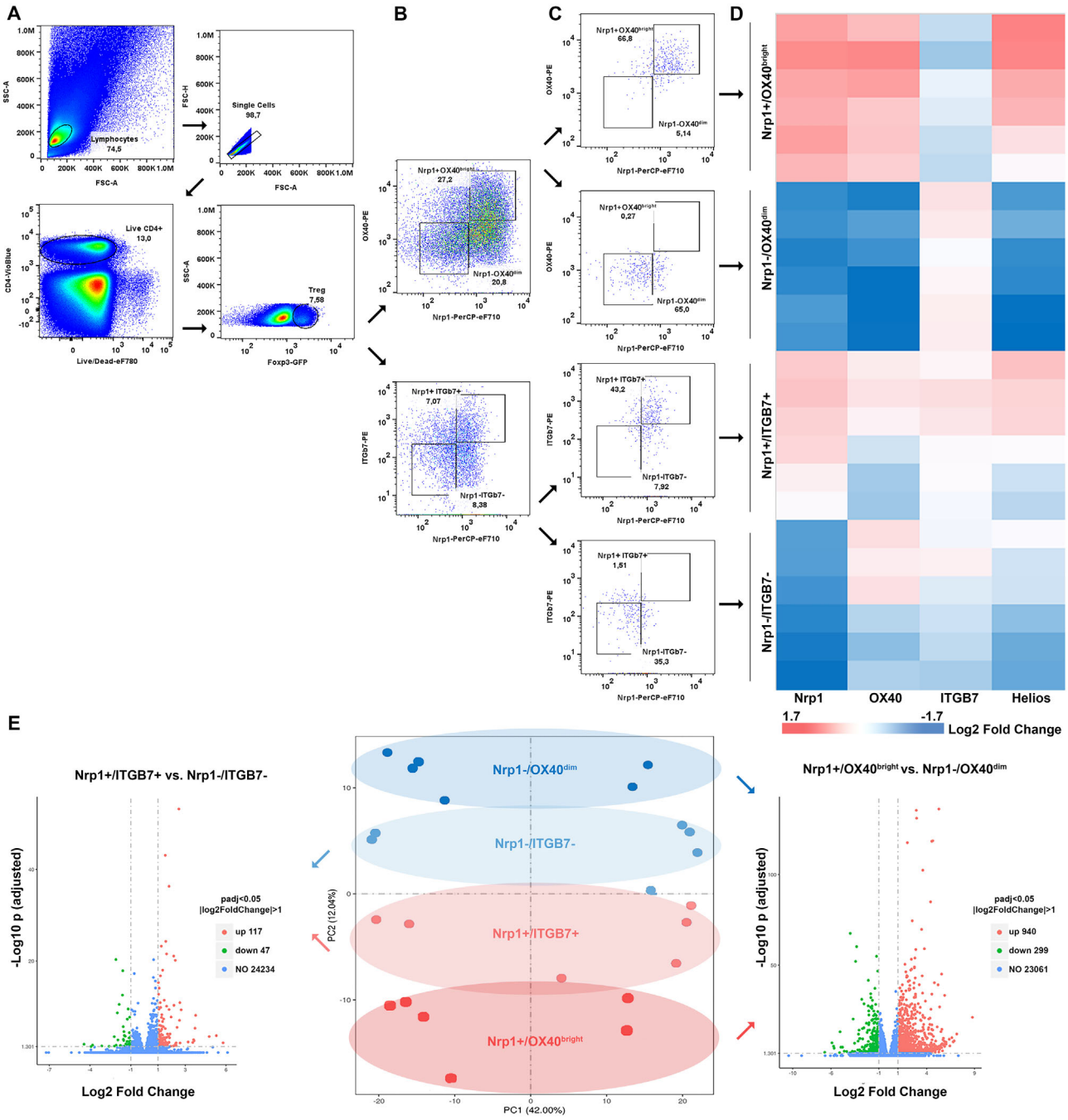

Figure 7. Fluorescence-activated cell sorter (FACS) sorting and comparative transcriptome profiling of select Treg subsets differentially affected by pretransplant conditioning in a healthy host. (Panel A) Representative data showing FACS sorting and transcriptome profiling of select splenic Treg subsets of a healthy host disproportionally affected by pretransplant conditioning. Gating strategies applied to sort host Ly/singlet/Live/CD4$^+$/Foxp3$^+$ Treg cells (Panel A) into Neuropilin-1 (Nrp1)$^+$/OX40^{bright} versus Nrp1$^-$/OX40^{dim} and Nrp1$^+$/integrin-β7 (ITGB7)$^+$ versus Nrp1$^-$/ITGB7$^-$ subsets (Panel B), followed by flow cytometry as purity assessment (Panel C) and transcriptome profiling showing messenger RNA (mRNA) levels of Nrp1, OX40, ITGB7, and Helios mRNA expression in the four subsets (Panel D). Principal component analysis (PCA) confirms sorting marker expression as a principal component of variance (Panel E), markedly affecting the gene expression profile of the four subsets. Volcano plots displaying the number of differentially affected genes, distribution of fold change, and significance (multiple testing corrected) obtained by comparing the four subsets in a pairwise manner. Results of one experiment, $n = 6$, log2 fold change (FC) and p-values shown, the latter calculated using a negative binomial distribution model, corrected by the Benjamini–Hochberg method for multiple testing.

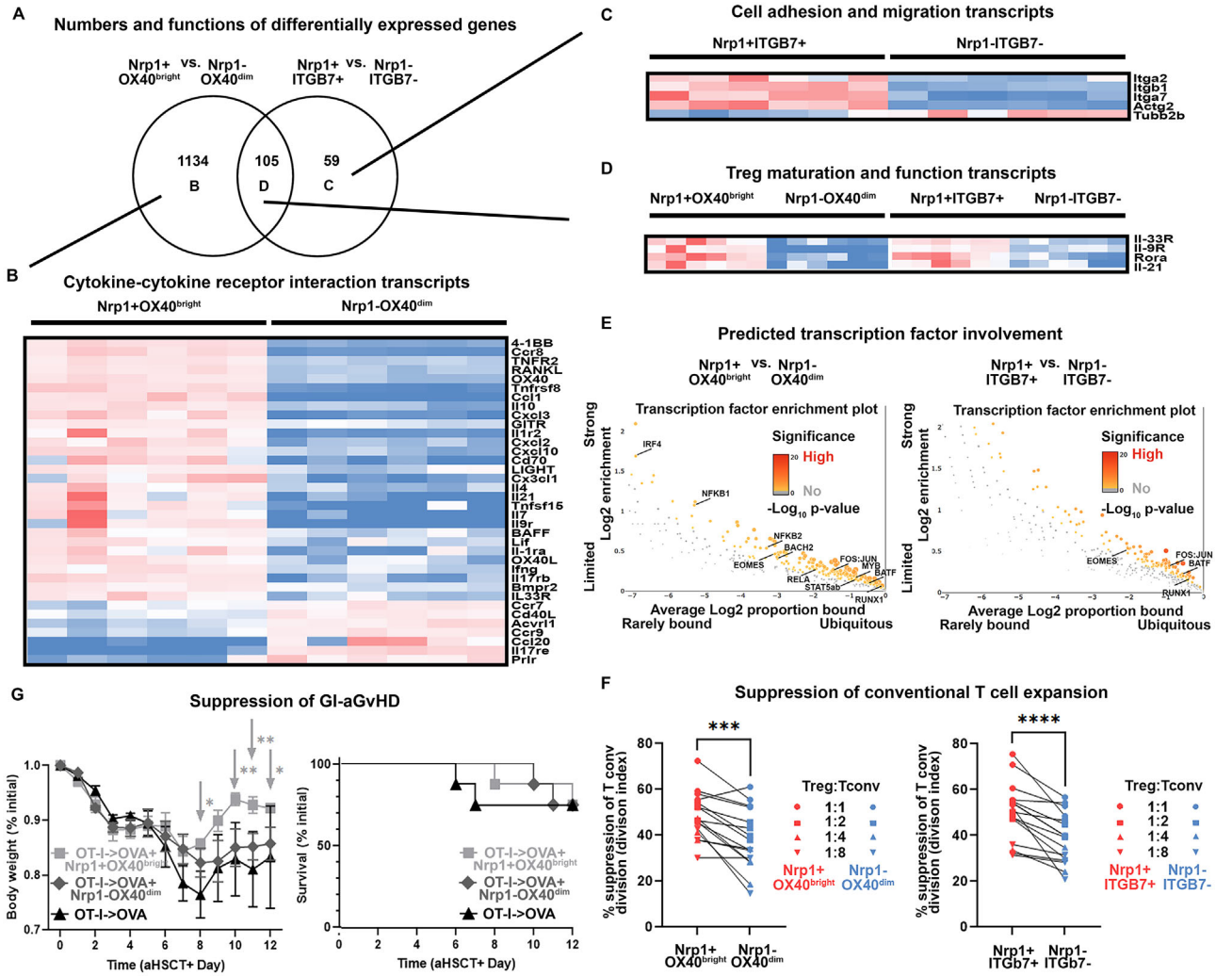

Figure 8. Functional analysis and suppressive activity of a healthy host's Treg subsets most affected by pretransplant conditioning and subsequent gastrointestinal acute graft versus host disease (GI-aGVHD). Gene expression profiling of four Treg subsets most affected in pretransplant conditioning by radiation, and in subsequent GI-aGVHD. Number (Panel A) and functional enrichment of Treg messenger RNA (mRNA) transcripts (Panels B–D) differentially expressed by Neuropilin-1 (Nrp1)$^{+}$/OX40^{bright} versus. Nrp1^{-}/OX40^{dim} Treg (see Panel B for select examples), Nrp1^{+}/integrin-β7 (ITGB7)$^{+}$ versus Nrp1^{-}/ITGb7^{-} Treg (see Panel C for select examples), or behaving identically in both comparisons (see Panel D for select examples). (Panel A) The Venn diagram displays the number of differentially expressed genes (DEGs) in each comparison. (Panels B–D) Heatmaps show patterns of gene expression in each indicated Treg subset; transcripts are identified by their respective gene symbols. Results of one experiment, $n = 6$; all markers shown display ≥1 log2 fold change, and Benjamini–Hochberg corrected significant difference between gene expression levels, $p < 0.05$. (Panel E) Treg-related transcription factors with binding sites significantly enriched in the promoter regions of the DEGs shown in Panels (B)–(D). Output of a CiiiDER analysis; binding frequency, enrichment, and significance are shown on the axes of the dot plots, and by color code, respectively. (Panel F) Analysis of the in vitro suppressive activity of Treg subsets shown above. Sorted live Treg subsets were cocultured with conventional CD8^{+} T cells in live Treg suppression assays at the Treg-conventional T cell (Tconv) ratios indicated. Nrp1^{+}/OX40^{bright} Treg display superior suppression of the clonal expansion of conventional CD8^{+} T cells as compared to versus Nrp1^{-}/OX40^{dim} Treg. Similar differences found between Nrp1^{+}/ITGB7^{+} Treg versus Nrp1^{-}/ITGb7^{-} Treg. Paired dot plots display results of two independent experiments, $n = 4$ each, paired t-test, stars indicate significance, $^{***}p < 0.001$, $^{****}p < 0.0001$). (Panel G) Exploratory analysis of the efficacy of Nrp1^{+}/OX40^{bright} versus Nrp1^{-}/OX40^{dim} Treg cells coadministered with the OT-I graft to OVA hosts as GvHD prophylaxis (pale gray, dark gray, respectively). OT-I grafts administered to OVA mice without Treg were used as reference (black). Results of two independent experiments, $n = 4$ each. Weight loss and survival analyzed by the mixed effects model and Kaplan–Meier survival analysis, respectively. Color-coded stars indicate significant difference between the given Treg prophylaxis and OT-I graft treatment, as reference; $^{*}p < 0.05$, $^{**}p < 0.01$. The weight loss graph displays daily changes in body weight of the experimental groups indicated, mean and SEM, compared to initial (percent). The Kaplan–Meier plot shows overall survival in the same groups (percent).

subpopulations that clearly share some relevant functional characteristics, such as superior T-cell suppressive activity.

Considering this, and the fact that Nrp1/OX40 status was clearly superior to Nrp1/ITGB7 at affecting the transcriptional Treg phenotype, we finally tested whether Ly/singlet/Foxp3^{+}/Nrp1^{+}/OX40^{bright} and Ly/singlet/Foxp3^{+}/Nrp1^{-}/OX40^{dim} Treg cells, coadministered with the graft as GvHD prophylaxis, would have different effects on the subsequent disease

course of murine experimental GI-aGvHD. This in vivo GvHD suppression assay demonstrated that coadministration of Ly/singlet/Foxp3$^+$/Nrp1$^+$/OX40^{bright} Treg with the graft resulted in significant suppression of GI-aGvHD as compared to that of Ly/singlet/Foxp3$^+$/Nrp1$^-$/OX40^{dim} Treg. An Ly/singlet/Foxp3$^+$/Nrp1$^+$/OX40^{bright} Treg-based prophylaxis resulted in limited weight loss and faster recovery among surviving animals, in a time-dependent manner, beginning from day 8 post-aHSCT ($p = 0.0057$, Fig. 8G). In contrast, Ly/singlet/Foxp3$^+$/Nrp1$^-$/OX40^{dim} Treg had only marginal benefit, and this difference did not reach significance at any of the time points investigated (Fig. 8G). On the other hand, there was no significant difference between the overall survival of mice receiving Ly/singlet/Foxp3$^+$/Nrp1$^+$/OX40^{bright} and Ly/singlet/Foxp3$^+$/Nrp1$^-$/OX40^{dim} Treg cells as prophylaxis.

Discussion

Depletion and functional impairment of Treg cells by conditioning before aHSCT and in subsequent aGVHD are well-known phenomena, the existence and clinical relevance of which are supported by multiple lines of evidence. In patients undergoing aHSCT, low circulating Treg count at 30 days after transplantation was found to correlate with increased risk to develop severe GvHD [14]. Further, it was shown that at the onset of aGvHD, affected patients have lower Treg/Tconv ratio than patients without aGvHD [58]. Finally, it has been suggested that in aGVHD, Treg homing to the gut is hampered, contributing to local Treg dysfunction and widespread inflammation caused by the conditioning regimen [59–61]. Inspired by these and similar reports, a multitude of studies analyzed the prophylactic and therapeutic efficacy of adoptive transfer, expansion, activation, or functional modification of Treg cells in murine models, humanized murine models, and human aGvHD. These studies confirmed that administration of functionally intact Treg unaffected by conditioning, expansion and stabilization of Treg after conditioning, or redirection of Treg to the gut or inflamed tissues are promising treatment strategies clearly capable of suppressing the development of aGvHD [13, 62–65].

Here we show that the balance of Treg subsets of a murine host, expressing both Nrp1 and Helios simultaneously, or none of them, is markedly offset by pretransplant conditioning performed as TBI before aHSCT. Conditioning results in a decreased relative frequency of Nrp1$^+$/Helios$^+$ Treg in clear favor of Nrp1$^-$/Helios$^-$ Treg cells, whereas single-positive Treg remain largely unaffected. We also demonstrate that upon addition of an allogeneic graft, that is in GI-aGvHD, Treg expressing Nrp1 and Helios respond to graft-mediated gut damage by upregulation of OX40 and ITGB7, whereas Treg that do not are incapable of such a response. We further analyzed the link between induced ITGB7 and OX40 expressions, and Nrp1 and Helios, for several reasons. First, the elevated expression of ITGB7 is a well-known marker of the commitment to gut homing on T cells, which has not yet been analyzed in the context of these two markers in aGvHD, however. Second, although the influence of OX40 ligand binding on Treg stability and activity has been studied in depth, with landmark studies showing that activation of OX40 may heavily interfere with Treg differentiation, Foxp3 expression, and IL-10 production [66, 67], others noted that in OX40$^+$ Treg may be superior to their OX40$^-$ counterparts in terms of T-cell suppressive capacity [68], and systematic reviews concluded that the net effect of OX40 signaling on Treg remains an elusive issue, as it depends on the Treg subset affected, tissue localization, timing and strength of the signal mediated by OX40, and various external factors [69]. In particular, several conflicting observations have been made in the context of radiation-mediated lymphodepletion in conditioning and subsequent aGvHD, either supporting, questioning, or challenging the notion that OX40 may interfere with activity and survival of Treg in these settings [70–73]. Indeed, NGS-based transcriptome analysis linked adhesion and migration-related mRNA transcripts to ITGB7, whereas the composition of mRNA transcripts related to the presence of OX40 seems to reflect the above detailed ambiguity of OX40 as a biomarker on Treg in the context of aHSCT and GvHD.

Of note, conditioning- and GvHD-specific differences observed in this study occurred in a largely tissue-independent manner, system-wide, suggesting a limited influence of the local tissue environment on them. This was in marked contrast with the behavior of other Treg markers studied, showing tissue-restricted differences in Treg marker expression (CD39) or interactions between tissue environment and external stressors, such as aHSCT followed by GI-aGvHD (LAP/TGFb, LAG3).

Taken together, our data suggest that conditioning by irradiation affects several Treg subsets of the host characteristically, unlike radiation-dependent gut damage in experimental colitis, or allograft-induced gut damage in GI-aGVHD, but they also underline clear differences between them. The net effect of conditioning is a relative shrinkage of Nrp1$^+$/Helios$^+$ Treg subsets capable of enhancing OX40 and ITGB7 protein expression in GI-GvHD, expressing a large array of mRNA transcripts functionally related to Treg activation, cell migration, and adhesion, and less efficient control of clonal Tconv expansion by Treg cells of the host.

In light of the above, and the well-documented Treg dysfunctionality in aGvHD, we suggest that Treg expressing Nrp1 and Helios are highly sensitive and responsive to the development of aGvHD. Unfortunately, the very same subset is more prone to conditioning-mediated shrinkage than Treg that do not express these markers, the net effect of which is that pretransplant conditioning limits commitment to gut homing of Treg and hampers control of CD8$^+$ T-cell expansion in posttransplant GVHD by Treg cells. Of note, the suggestion that Nrp1-expressing Treg may be disproportionally affected by radiation-mediated stress is not without precedent [38], and our data are in line with the reported ambiguity of the net effect of OX40 signaling on Treg function after conditioning, and in aGvHD developed upon aHSCT [69, 70, 73]. Finally, our data provide proof-of-concept that a better understanding of conditioning-induced changes affecting host Treg subsets may be exploited in the optimization of Treg-based GvHD prophylaxis. Nevertheless, the applicability of these

findings to human GvHD, the feasibility of selecting or expanding Treg subsets based on these criteria for prophylaxis, and the clinical usefulness of such prophylactic regimens require further careful evaluation.

Further studies are warranted to analyze the behavior of these Treg subsets in other, independent murine aGvHD models, as well, such as other minor (miHA) and major (MHC) antigen mismatch-based models, in both genders, in human patients, and under the influence of cofounding factors such as genetic heterogeneity, or age- and gender-related differences in Treg behavior. First and foremost, however, these Treg subsets need to be studied under the influence of other, radiation-independent conditioning regimens used either in combination with or alternatively to TBI in the treatment of patients undergoing aHSCT. It is conceivable that myeloablative, nonmyeloablative, and reduced intensity conditioning, using various regimens of chemotherapy, either alone or in combination with radio- or T-cell suppressive immunotherapy, may influence host Treg subsets in different ways. A better understanding of the interactions between host Treg subsets and distinct conditioning regimens may aid optimalization of the Treg products currently used for GvHD prophylaxis and therapy, as it may help reconstitution of lost Treg functions in a more patient-specific, personalized manner, also reflecting to the applied conditioning regimen.

Methodical standards

These studies were conducted in an ISO 9001:2015-certified laboratory that operates under exploratory research principles. All studies were performed using established laboratory protocols and research assays. FACS sorting and flow cytometry were performed following the 'Guidelines for the use of flow cytometry and cell sorting in immunological studies' [74].

Acknowledgements: This work was supported by the National Research, Development, and Innovation Office (Grants K 131627 to ZP, and FK 138842 to ZZ).

Conflict of interest: The authors declare that there are no financial or commercial conflicts of interest.

Author contributions: Katalin Lumniczky, Géza Sáfrány, Edit I Buzás, Zoltán S Zádori, and Zoltán Pós contributed to conception and design of the study. Nikolett Lupsa, Barbara Érsek, Csenge Böröczky, and Zoltán Pós collected the data. Dávid Kis, Eszter Szarka, Zoltán S Zádori, and Árpád Szöőr contributed analysis tools. Nikolett Lupsa, Barbara Érsek, and Zoltán Pós analyzed data and performed statistical analysis. Zoltán Pós wrote the first draft of the manuscript. LN and Barbara Érsek wrote sections of the manuscript. All authors contributed to manuscript revision, read, and approved the submitted version.

Ethics statement: All animal experiments were conducted with the approval of the Institutional Animal Care and Use Committee, the National Scientific Ethical Committee on Animal Experimentation, and permitted by the Food Chain Safety and Animal Health Directorate of the Government Office (permissions PE/EA/631-8-2018 and PE/EA/00611-6/2022 to ZP).

Data availability statement: Gene expression data that support the findings of this study are openly available in GEO at https://www.ncbi.nlm.nih.gov/geo/, reference number GSE227929. Flow cytometry data that support the findings of this study are available from the corresponding author upon reasonable request.

Peer review: The peer review history for this article is available at https://publons.com/publon/10.1002/eji.202350619.

References

1 **Aladag, E., Kelkitli, E. and Goker, H.**, Acute graft-versus-host disease: a brief review. *Turk. J. Haematol.* 2020. **37**: 1–4.

2 **Ara, T. and Hashimoto, D.**, Novel insights into the mechanism of GVHD-induced tissue damage. *Front. Immunol.* 2021. **12**: 713631.

3 **Ramachandran, V., Kolli, S. S. and Strowd, L. C.**, Review of graft-versus-host disease. *Dermatol. Clin.* 2019. **37**: 569–582.

4 **Zeiser, R. and Teshima, T.**, Nonclassical manifestations of acute GVHD. *Blood* 2021. **138**: 2165–2172.

5 **Thangavelu, G. and Blazar, B. R.**, Achievement of tolerance induction to prevent acute graft-vs.-host disease. *Front. Immunol.* 2019. **10**: 309.

6 **Ferrara, J. L., Smith, C. M., Sheets, J., Reddy, P. and Serody, J. S.**, Altered homeostatic regulation of innate and adaptive immunity in lower gastrointestinal tract GVHD pathogenesis. *J. Clin. Invest.* 2017. **127**: 2441–2451.

7 **Li, A., Abraham, C., Wang, Y. and Zhang, Y.**, New insights into the basic biology of acute graft-versus-host-disease. *Haematologica* 2020. **105**: 2540–2549.

8 **Sefik, E., Geva-Zatorsky, N., Oh, S., Konnikova, L., Zemmour, D., McGuire, A. M., Burzyn, D. et al.**, Mucosal immunology. Individual intestinal symbionts induce a distinct population of ROR gamma (+) regulatory T cells. *Science* 2015. **349**: 993–997.

9 **Zeiser, R. and Blazar, B. R.**, Preclinical models of acute and chronic graft-versus-host disease: how predictive are they for a successful clinical translation? *Blood* 2016. **127**: 3117–3126.

10 **Boieri, M., Shah, P., Dressel, R. and Inngjerdingen, M.**, The role of animal models in the study of hematopoietic stem cell transplantation and GvHD: a historical overview. *Front. Immunol.* 2016. **7**: 333.

11 **Teshima, T. and Hill, G. R.**, The pathophysiology and treatment of graft-versus-host disease: lessons learnt from animal models. *Front. Immunol.* 2021. **12**: 715424.

12 **Khan, U. and Ghazanfar, H.**, T lymphocytes and autoimmunity. *Int. Rev. Cell Mol. Biol.* 2018. **341**: 125–168.

13 **Guo, W. W., Su, X. H., Wang, M. Y., Han, M. Z., Feng, X. M. and Jiang, E. L.**, Regulatory T cells in GVHD therapy. *Front. Immunol.* 2021. **12**: 697854.

14 **Whangbo, J. S., Antin, J. H. and Koreth, J.**, The role of regulatory T cells in graft-versus-host disease management. *Expert Rev. Hematol.* 2020. **13**: 141–154.

15 **Huehn, J. and Beyer, M.**, Epigenetic and transcriptional control of Foxp3+ regulatory T cells. *Semin. Immunol.* 2015. **27**: 10–18.

16 **Sakai, R., Komai, K., Iizuka-Koga, M., Yoshimura, A. and Ito, M.**, Regulatory T Cells: pathophysiological roles and clinical applications. *Keio J. Med.* 2020. **69**: 1–15.

17 **Sakaguchi, S., Mikami, N., Wing, J. B., Tanaka, A., Ichiyama, K. and Ohkura, N.**, Regulatory T cells and human disease. *Annu. Rev. Immunol.* 2020. **38**: 541–566.

18 **Sznurkowska, K., Zawrocki, A., Sznurkowski, J., Izycka-Swieszewska, E., Landowski, P., Szlagatys-Sidorkiewicz, A., Plata-Nazar, K. et al.**, Indoleamine 2,3-dioxygenase and regulatory t cells in intestinal mucosa in children with inflammatory bowel disease. *J. Biol. Regul. Homeost. Agents* 2017. **31**: 125–131.

19 **van Herk, E. H.**, and **Te Velde, A. A.**, Treg subsets in inflammatory bowel disease and colorectal carcinoma: characteristics, role, and therapeutic targets. *J. Gastroenterol. Hepatol.* 2016. **31**: 1393–1404.

20 **Pedros, C., Duguet, F., Saoudi, A. and Chabod, M.**, Disrupted regulatory T cell homeostasis in inflammatory bowel diseases. *World J. Gastroenterol.* 2016. **22**: 974–995.

21 **Thornton, A. M., Lu, J., Korty, P. E., Kim, Y. C., Martens, C., Sun, P. D. and Shevach, E. M.**, Helios(+) and Helios(-) Treg subpopulations are phenotypically and functionally distinct and express dissimilar TCR repertoires. *Eur. J. Immunol.* 2019. **49**: 398–412.

22 **Chen, W. Q., Huang, W. S., Xue, Y. Q., Chen, Y., Qian, W. B., Ma, J. L., August, A. et al.**, Neuropilin-1 identifies a new subpopulation of TGF-beta-induced Foxp3(+) regulatory T cells with potent suppressive function and enhanced stability during inflammation. *Front. Immunol.* 2022. **13**: 900139.

23 **Tanoue, T., Atarashi, K. and Honda, K.**, Development and maintenance of intestinal regulatory T cells. *Nat. Rev. Immunol.* 2016. **16**: 295–309.

24 **Thornton, A. M., Korty, P. E., Tran, D. Q., Wohlfert, E. A., Murray, P. E., Belkaid, Y. and Shevach, E. M.**, Expression of Helios, an Ikaros transcription factor family member, differentiates thymic-derived from peripherally induced Foxp3+ T regulatory cells. *J. Immunol.* 2010. **184**: 3433–3441.

25 **Weiss, J. M., Bilate, A. M., Gobert, M., Ding, Y., Curotto de Lafaille, M. A., Parkhurst, C. N., Xiong, H. et al.**, Neuropilin 1 is expressed on thymus-derived natural regulatory T cells, but not mucosa-generated induced Foxp3+ T reg cells. *J. Exp. Med.* 2012. **209**: 1723–1742, S1721.

26 **Yadav, M., Louvet, C., Davini, D., Gardner, J. M., Martinez-Llordella, M., Bailey-Bucktrout, S., Anthony, B. A. et al.**, Neuropilin-1 distinguishes natural and inducible regulatory T cells among regulatory T cell subsets in vivo. *J. Exp. Med.* 2012. **209**: 1713–1722, S1711–1719.

27 **Chen, W., Huang, W., Xue, Y., Chen, Y., Qian, W., Ma, J., August, A. et al.**, Neuropilin-1 identifies a new subpopulation of TGF-beta-induced Foxp3(+) regulatory T cells with potent suppressive function and enhanced stability during inflammation. *Front. Immunol.* 2022. **13**: 900139.

28 **Shevach, E. M. and Thornton, A. M.**, tTregs, pTregs, and iTregs: similarities and differences. *Immunol. Rev.* 2014. **259**: 88–102.

29 **MacDonald, K. G., Han, J. M., Himmel, M. E., Huang, Q., Kan, B., Campbell, A. I., Lavoie, P. M. et al.**, Response to comment on "helios+ and helios- cells coexist within the natural FOXP3+ T regulatory cell subset in humans". *J. Immunol.* 2013. **190**: 4440–4441.

30 **Akimova, T., Beier, U. H., Wang, L., Levine, M. H. and Hancock, W. W.**, Helios expression is a marker of T cell activation and proliferation. *PLoS One* 2011. **6**: e24226.

31 **Serre, K., Benezech, C., Desanti, G., Bobat, S., Toellner, K. M., Bird, R., Chan, S. et al.**, Helios is associated with CD4 T cells differentiating to T helper 2 and follicular helper T cells in vivo independently of Foxp3 expression. *PLoS One* 2011. **6**: e20731.

32 **Lam, A. J., Uday, P., Gillies, J. K. and Levings, M. K.**, Helios is a marker, not a driver, of human Treg stability. *Eur. J. Immunol.* 2022. **52**: 75–84.

33 **Sebastian, M., Lopez-Ocasio, M., Metidji, A., Rieder, S. A., Shevach, E. M. and Thornton, A. M.**, Helios controls a limited subset of regulatory T cell functions. *J. Immunol.* 2016. **196**: 144–155.

34 **Bruder, D., Probst-Kepper, M., Westendorf, A. M., Geffers, R., Beissert, S., Loser, K., von Boehmer, H. et al.**, Neuropilin-1: a surface marker of regulatory T cells. *Eur. J. Immunol.* 2004. **34**: 623–630.

35 **Delgoffe, G. M., Woo, S. R., Turnis, M. E., Gravano, D. M., Guy, C., Overacre, A. E., Bettini, M. L. et al.**, Stability and function of regulatory T cells is maintained by a neuropilin-1-semaphorin-4a axis. *Nature* 2013. **501**: 252–256.

36 **Sarris, M., Andersen, K. G., Randow, F., Mayr, L. and Betz, A. G.**, Neuropilin-1 expression on regulatory T cells enhances their interactions with dendritic cells during antigen recognition. *Immunity* 2008. **28**: 402–413.

37 **Hansen, W., Hutzler, M., Abel, S., Alter, C., Stockmann, C., Kliche, S., Albert, J. et al.**, Neuropilin 1 deficiency on CD4+Foxp3+ regulatory T cells impairs mouse melanoma growth. *J. Exp. Med.* 2012. **209**: 2001–2016.

38 **Battaglia, A., Buzzonetti, A., Monego, G., Peri, L., Ferrandina, G., Fanfani, F., Scambia, G. et al.**, Neuropilin-1 expression identifies a subset of regulatory T cells in human lymph nodes that is modulated by preoperative chemoradiation therapy in cervical cancer. *Immunology* 2008. **123**: 129–138.

39 **Ersek, B., Lupsa, N., Pocza, P., Toth, A., Horvath, A., Molnar, V., Bagita, B. et al.**, Unique patterns of CD8+ T-cell-mediated organ damage in the Act-mOVA/OT-I model of acute graft-versus-host disease. *Cell. Mol. Life Sci.* 2016. **73**: 3935–3947.

40 **Gearing, L. J., Cumming, H. E., Chapman, R., Finkel, A. M., Woodhouse, I. B., Luu, K., Gould, J. A. et al.**, CiiiDER: a tool for predicting and analysing transcription factor binding sites. *PLoS One* 2019. **14**: e0215495.

41 **Castro-Mondragon, J. A., Riudavets-Puig, R., Rauluseviciute, I., Lemma, R. B., Turchi, L., Blanc-Mathieu, R., Lucas, J. et al.**, JASPAR 2022: the 9th release of the open-access database of transcription factor binding profiles. *Nucleic. Acids. Res.* 2022. **50**: D165–D173.

42 **Janetzki, S., Britten, C. M., Kalos, M., Levitsky, H. I., Maecker, H. T., Melief, C. J., Old, L. J. et al.**, "MIATA"-minimal information about T cell assays. *Immunity* 2009. **31**: 527–528.

43 **Mortazavi, A., Williams, B. A., McCue, K., Schaeffer, L. and Wold, B.**, Mapping and quantifying mammalian transcriptomes by RNA-Seq. *Nat. Methods* 2008. **5**: 621–628.

44 **Love, M. I., Huber, W. and Anders, S.**, Moderated estimation of fold change and dispersion for RNA-seq data with DESeq2. *Genome Biol.* 2014. **15**: 550.

45 **Benjamini, Y. and Hochberg, Y.**, Controlling the false discovery rate: a practical and powerful approach to multiple testing. *J. R. Stat. Soc. Series B (Methodological)* 1995. **57**: 289–300.

46 **Luke, J. J., Zha, Y., Matijevich, K. and Gajewski, T. F.**, Single dose denileukin diftitox does not enhance vaccine-induced T cell responses or effectively deplete Tregs in advanced melanoma: immune monitoring and clinical results of a randomized phase II trial. *J. Immunother. Cancer* 2016. **4**: 35.

47 **Zhu, K., He, C., Liu, S. Q., Qu, M., Xie, T., Yang, X., Lei, L. et al.**, Lineage tracking the generation of T regulatory cells from microbial activated T effector cells in naive mice. *Front. Immunol.* 2019. **10**: 3109.

48 **Zhou, X., Wang, J., Shi, W., Brand, D. D., Liu, Z., Fan, H. and Zheng, S. G.**, Isolation of purified and live Foxp3+ regulatory T cells using FACS sorting on scatter plot. *J. Mol. Cell Biol.* 2010. **2**: 164–169.

49 **Siede, J., Frohlich, A., Datsi, A., Hegazy, A. N., Varga, D. V., Holecska, V., Saito, H. et al.**, IL-33 receptor-expressing regulatory T cells are highly activated, Th2 biased and suppress CD4 T cell proliferation through IL-10 and TGFbeta release. *PLoS One* 2016. **11**: e0161507.

50 **Pastille, E., Wasmer, M. H., Adamczyk, A., Vu, V. P., Mager, L. F., Phuong, N. N. T., Palmieri, V. et al.**, The IL-33/ST2 pathway shapes the regulatory

T cell phenotype to promote intestinal cancer. *Mucosal. Immunol.* 2019. **12**: 990–1003.

51 **Heim, L., Yang, Z., Tausche, P., Hohenberger, K., Chiriac, M. T., Koelle, J., Geppert, C. I. et al.**, IL-9 producing tumor-infiltrating lymphocytes and Treg subsets drive immune escape of tumor cells in non-small cell lung cancer. *Front. Immunol.* 2022. **13**: 859738.

52 **Elyaman, W., Bradshaw, E. M., Uyttenhove, C., Dardalhon, V., Awasthi, A., Imitola, J., Bettelli, E. et al.**, IL-9 induces differentiation of TH17 cells and enhances function of FoxP3+ natural regulatory T cells. *Proc. Natl. Acad. Sci. USA* 2009. **106**: 12885–12890.

53 **Malhotra, N., Leyva-Castillo, J. M., Jadhav, U., Barreiro, O., Kam, C., O'Neill, N. K., Meylan, F. et al.**, RORalpha-expressing T regulatory cells restrain allergic skin inflammation. *Sci. Immunol.* 2018. **3**: eaao6923.

54 **Dempsey, L. A.**, RORα in Treg cells. *Nat. Immunol.* 2018. **19**: 510–510.

55 **Spolski, R., Kim, H. P., Zhu, W., Levy, D. E. and Leonard, W. J.**, IL-21 mediates suppressive effects via its induction of IL-10. *J. Immunol.* 2009. **182**: 2859–2867.

56 **Ono, M.**, Control of regulatory T-cell differentiation and function by T-cell receptor signalling and Foxp3 transcription factor complexes. *Immunology* 2020. **160**: 24–37.

57 **Cretney, E., Kallies, A. and Nutt, S. L.**, Differentiation and function of Foxp3(+) effector regulatory T cells. *Trends Immunol.* 2013. **34**: 74–80.

58 **Magenau, J. M., Qin, X., Tawara, I., Rogers, C. E., Kitko, C., Schlough, M., Bickley, D. et al.**, Frequency of CD4(+)CD25(hi)FOXP3(+) regulatory T cells has diagnostic and prognostic value as a biomarker for acute graft-versus-host-disease. *Biol. Blood Marrow Transplant.* 2010. **16**: 907–914.

59 **Engelhardt, B. G., Jagasia, M., Savani, B. N., Bratcher, N. L., Greer, J. P., Jiang, A., Kassim, A. A. et al.**, Regulatory T cell expression of CLA or alpha(4)beta(7) and skin or gut acute GVHD outcomes. *Bone Marrow Transplant.* 2011. **46**: 436–442.

60 **Engelhardt, B. G., Sengsayadeth, S. M., Jagasia, M., Savani, B. N., Kassim, A. A., Lu, P., Shyr, Y. et al.**, Tissue-specific regulatory T cells: biomarker for acute graft-vs-host disease and survival. *Exp. Hematol.* 2012. **40**: 974–982 e971.

61 **Engelhardt, B. G. and Crowe, J. E. Jr.**, Homing in on acute graft vs. host disease: tissue-specific T regulatory and Th17 cells. *Curr. Top. Microbiol. Immunol.* 2010. **341**: 121–146.

62 **Blazar, B. R., MacDonald, K. P. A. and Hill, G. R.**, Immune regulatory cell infusion for graft-versus-host disease prevention and therapy. *Blood* 2018. **131**: 2651–2660.

63 **Ramlal, R. and Hildebrandt, G. C.**, Advances in the use of regulatory T-cells for the prevention and therapy of Graft-vs.-host disease. *Biomedicines* 2017. **5**: 23.

64 **Rezvani, K., Mielke, S., Ahmadzadeh, M., Kilical, Y., Savani, B. N., Zeilah, J., Keyvanfar, K. et al.**, High donor FOXP3-positive regulatory T-cell (Treg) content is associated with a low risk of GVHD following HLA-matched allogeneic SCT. *Blood* 2006. **108**: 1291–1297.

65 **Hoeppli, R. E., MacDonald, K. N., Leclair, P., Fung, V. C. W., Mojibian, M., Gillies, J., Rahavi, S. M. R. et al.**, Tailoring the homing capacity of human Tregs for directed migration to sites of Th1-inflammation or intestinal regions. *Am. J. Transplant.* 2019. **19**: 62–76.

66 **Zhang, X., Xiao, X., Lan, P., Li, J., Dou, Y., Chen, W., Ishii, N. et al.**, OX40 costimulation inhibits Foxp3 expression and treg induction via BATF3-dependent and independent mechanisms. *Cell Rep.* 2018. **24**: 607–618.

67 **Ito, T., Wang, Y. H., Duramad, O., Hanabuchi, S., Perng, O. A., Gilliet, M., Qin, F. X. et al.**, OX40 ligand shuts down IL-10-producing regulatory T cells. *Proc. Natl. Acad. Sci. USA* 2006. **103**: 13138–13143.

68 **Piconese, S., Timperi, E. and Barnaba, V.**, 'Hardcore' OX40(+) immunosuppressive regulatory T cells in hepatic cirrhosis and cancer. *Oncoimmunology* 2014. **3**: e29257.

69 **Willoughby, J., Griffiths, J., Tews, I. and Cragg, M. S.**, OX40: structure and function - what questions remain? *Mol. Immunol.* 2017. **83**: 13–22.

70 **Piconese, S., Pittoni, P., Burocchi, A., Gorzanelli, A., Care, A., Tripodo, C. and Colombo, M. P.**, A non-redundant role for OX40 in the competitive fitness of Treg in response to IL-2. *Eur. J. Immunol.* 2010. **40**: 2902–2913.

71 **Miura, Y., Thoburn, C. J., Bright, E. C., Arai, S. and Hess, A. D.**, Regulation of OX40 gene expression in graft-versus-host disease. *Transplant. Proc.* 2005. **37**: 57–61.

72 **Tkachev, V., Furlan, S. N., Watkins, B., Hunt, D. J., Zheng, H. B., Panoskaltsis-Mortari, A., Betz, K. et al.**, Combined OX40L and mTOR blockade controls effector T cell activation while preserving T(reg) reconstitution after transplant. *Sci. Transl. Med.* 2017. **9**: eaan3085.

73 **Tripathi, T., Yin, W., Xue, Y., Zurawski, S., Fujita, H., Hanabuchi, S., Liu, Y. J. et al.**, Central roles of OX40L-OX40 interaction in the induction and progression of human T cell-driven acute graft-versus-host disease. *Immunohorizons* 2019. **3**: 110–120.

74 **Cossarizza, A., Chang, H. D., Radbruch, A., Acs, A., Adam, D., Adam-Klages, S., Agace, W. W. et al.**, Guidelines for the use of flow cytometry and cell sorting in immunological studies (second edition). *Eur. J. Immunol.* 2019. **49**: 1457–1973.

Abbreviations: **Act-mOVA**: transgenic actin beta promoter-controlled, membrane bound, chicken ovalbumin antigen · **aHSCT**: allogeneic hematopoietic stem cell transplantation · **ANOVA**: analysis of variance · **B6**: C57Bl/6/J · **CFSE**: carboxyfluorescein succinimidyl ester · **DEG**: differentially expressed gene · **DI**: division index · **DSS**: dextran sodium sulfate · **GFP**: green fluorescent protein · **GI-aGvHD**: gastrointestinal acute graft versus host disease · **GvHD**: graft versus host disease · **GZMA**: granzyme A · **GZMB**: granzyme B · **IBD**: inflammatory bowel disease · **ITGB7**: integrin-β7 · **LILP**: large intestinal lamina propria · **MLN**: mesenteric lymph nodes · **NGS**: next-generation sequencing · **Nrp1**: Neuropilin-1, CD304 · **OT-I**: murine $CD8^+$ Vα2/Vβ5 T-cell receptor specific for the chicken ovalbumin$^{257–264}$ antigen in the context of H-2Kb · **OX40**: CD134 · **PCA**: principal component analysis · **SILP**: small intestinal lamina propria · **TBI**: total body irradiation · **Tconv**: conventional T cell · **TF**: transcription factor · **Treg**: regulatory T cell

Full correspondence: Prof. Zoltán Pós, Associate Professor, Department of Genetics, Cell and Immunobiology, Semmelweis University, 4 Nagyvarad tér VII/709, Budapest 1089, Hungary
e-mail: pos.zoltan@semmelweis.hu

Received: 23/6/2023
Revised: 15/3/2024
Accepted: 18/3/2024
Accepted article online: 20/3/2024